Hindawi
International Journal of Aerospace Engineering
Volume 2022, Article ID 1601771, 19 pages
https://doi.org/10.1155/2022/1601771

Research Article

Observer-Based Robust Finite-Time Trajectory Tracking Control for a Stratospheric Satellite Subject to External Disturbance and Actuator Saturation

Shurui Huang,[1] Yueneng Yang,[1] Ye Yan,[2] Shifeng Zhang,[1] and Zhiyang Liu[1]

[1]*College of Aerospace Science and Engineering, National University of Defense Technology, Changsha, Hunan 410073, China*
[2]*National Innovation Institute of Defense Technology, Chinese Academy of Military Science, Beijing 100091, China*

Correspondence should be addressed to Yueneng Yang; yangyueneng@163.com

Received 22 August 2022; Revised 2 September 2022; Accepted 9 September 2022; Published 29 September 2022

Academic Editor: Xingling Shao

The stratospheric satellite is regarded as an ideal stratosphere flight platform and is able to accomplish various missions such as surveillance, earth observation, and remote sensing, which requires a robust and effective trajectory tracking control method to support these tasks. A novel observer-based robust finite-time control scheme is proposed to address the trajectory tracking control problem dedicated to a stratospheric satellite in the presence of external disturbance and actuator saturation. Firstly, an extended state observer (ESO) is adopted to observe the unavailable velocity states and unknown disturbances simultaneously, and the estimated data are utilized in the robust control law design. Then, an auxiliary system based on anti-windup compensator is developed to directly compensate for the actuator saturation difference. After that, a backstepping nonsingular fast terminal sliding mode control (BNFTSMC) strategy is designed to track the desired trajectory with high accuracy, fast convergence rate, and finite-time convergence. Then, a stability analysis using Lyapunov-based theory is performed, in which the stabilization of the stratospheric satellite system and finite-time convergence are proven. Furthermore, a number of simulations are conducted further to verify the excellent performance of the designed control strategy.

1. Introduction

Near space refers to the airspace 20-100 km above the earth surface, which is the transition between the highest flight height of traditional aircrafts and the lowest altitude orbit of low-Earth-orbit (LEO) satellites [1]. The stratosphere is at the bottom of near space and the most peaceful layer of the earth's atmosphere, which garners a great deal attention due to its stable meteorological condition [2, 3]. As a special lighter-than-air vehicle, the stratospheric airship is developed to operate in this zone for a long period; thus, it is called "stratospheric satellite." Compared with space-based satellites, the stratospheric satellite is capable of maneuvering to arbitrary positions without the restriction of orbit and has a shorter delay in receiving and transmitting signals [4]. Therefore, the stratospheric satellite performs better performance in aerial photography, scientific exploration, broadcasting relays, and remote sensing missions, to name just a few. To complete these complex tasks, it has research significance and practical value in developing the robust and effective control method for trajectory tracking dedicated to a stratospheric satellite, whereas the trajectory tracking controller design of a stratospheric satellite is a challenging task on account of the highly nonlinear, strong coupling, sensitivity to unknown external disturbances, and other factors.

To cope with the problem of motion control, a number of nonlinear control strategies have been successfully utilized in the stratospheric satellite, such as backstepping control [5, 6], adaptive control [7, 8], and sliding mode control (SMC) [9, 10]. Among the above methods, as a wildly used nonlinear control approach, the SMC method is regarded as a desirable control technique, which is low sensitivity towards dynamic uncertainties [11, 12]. Paiva et al. [13] proposed a SMC technique for the longitudinal control of an autonomous airship. Zheng and Sun [14] developed an adaptive

SMC for the airship with parameter uncertainties and unknown external disturbances. Yang et al. [15] presented a fuzzy adaptive SMC where the control gains are tuned based on the fuzzy logic system, for trajectory tracking control of an autonomous airship. Indeed, the conventional SMC method can only obtain the asymptotical convergence of the system states, but not in a limited time. To enhance the convergence performance and achieve the finite-time convergence, Wang et al. [16] developed a nonlinear finite-time control scheme proposed by combining the integral sliding mode technique with input/output feedback linearization. Considering the finite-time tracking control problem of a robotic airship, Cui et al. [17] designed a finite-time command-filtered backstepping supertwisting controller. Additionally, terminal sliding mode control (TSMC), adopting the nonlinear exponential sliding mode manifold, is developed to obtain the finite-time convergence, which has attracted considerable attention, whereas the traditional TSMC suffers from the singularity problem. To overcome this problem, Yang [18] proposed a time-specified nonsingular terminal sliding mode control (NTSMC) approach, dedicated to an autonomous unmanned airship, achieving singularity avoidance and finite-time convergence. Furthermore, TSMC is combined with a fuzzy logic system and neural network in Ref [19, 20], which reduces the dependence of the prior knowledge on the upper bound of the total system uncertainties and further improves the control performance. In order to further enhance the convergence speed, the nonsingular fast terminal sliding mode control (NFTSMC) method is developed, which has been applied in quadrotors [21], underwater vehicles [22], and spacecraft [23]. As far, there are few works utilizing NFTSMC strategy to address the trajectory tracking control problem of a stratospheric satellite. Therefore, in this research, a nonsingular fast terminal sliding mode (NFTSM) surface combined with backstepping technique, is selected to enhance the convergence speed and tracking precision.

The aforementioned works mainly concentrate on ensuring the robustness of the controller to handle the unknown system uncertainty. However, few of them explicitly consider the input saturation constraints. In fact, input saturation is intrinsically the physical constraint of the actuator, which means that the required force or torque is beyond the maximum force or torque that the stratospheric satellite can provide. If it is not treated appropriately, it may have an unfavorable effect on the system stability [24, 25]. There are several studies to cope with the input saturation problem of the control system. In order to address the input constraint problem, Gou et al. [26] combined a tan-type barrier Lyapunov function with the auxiliary variables. Based on the vectorial backstepping tracking controller, a control allocation module was designed to optimize the control inputs by the author of Ref. [27]. Yuan et al. [28] proposed a novel auxiliary system to solve the saturation problem and preserve the finite-time property. Chen et al. [29] introduced an auxiliary system in the form of a saturation compensator based on RBFNN to compensate for the possible saturation effect. Zheng et al. [30, 31] designed an anti-windup compensator to handle the input saturation effect. In addition, the anti-windup compensator combined with the backstepping approach provides more flexibility for addressing the actuator constraint problem, which is a recursive design procedure through the construction of Lyapunov functions. In this context, we employed an anti-windup compensator as the auxiliary system in the finite-time trajectory tracking control scheme for the stratospheric satellite to cope with the saturation problem.

Varieties of present studies on stratospheric satellite control are under the hypothesis that all state variables can be obtained directly. In general, due to the limitations of the stratospheric satellite sensors, the exact velocity states are difficult to measure by sensors precisely, and only the system output is available, including the position, attitude, and control input [32]. State observer can be utilized to online estimate the values of the velocity states, which can substantially reduce the cost, size, weight, and even noise of measuring them physically by using sensors [33–35]. Therefore, it is rather significant to design a suitable state observer to offer the necessary information to the controller design, and many researchers have done much work. In order to estimate the velocity state of the spacecraft system, Perruquetti et al. [36] proposed a nonlinear reduced-order observer for the spacecraft attitude control system. For path following control for a quadrotor, Meng et al. [37] constructed a full-order state observer to estimate the derivative of the quadrotor system output and a nonlinear disturbance observer to estimate the external disturbance. In terms of the observation gain, there are two kinds of ESO, linear ESO, and nonlinear ESO. Although the nonlinear ESO can obtain high tracking accuracy, its parameter adjustment is too complicated. The linear ESO has the merits of simple structure and good state estimation performance. At present, ESO for stratospheric satellite motion control is rarely studied by researchers. Inspired by Ref. [38], a third-order linear ESO is utilized to estimate the unmeasurable velocity states and unknown external disturbance.

Motivated by the above discussion, this paper proposed an observer-based robust finite-time controller, to settle the trajectory tracking control problem of the stratospheric satellite subject to external disturbances and actuator saturation. In order to dispose of the unknown external disturbance, based on the NFTSM surface, a novel backstepping nonsingular fast terminal sliding mode control (BNFTSMC) method is proposed. The designed BNFTSMC strategy takes advantages of backstepping technique and NFTSMC technique. On the one hand, the BNFTSMC improves the convergence rate of system state and does not exhibit any singularity problem. On the other hand, the design topology follows the design procedure of backstepping strategy and the global stability of the closed-loop system is ensured. In addition, the position and velocity tracking errors can obtain the finite-time convergence to small regions around zero. For the input saturation constraint, an assistant system based on the anti-windup compensator is formulated to compensate for the saturation effect. Furthermore, an ESO is adopted to estimate the unmeasurable state variables and external interferences simultaneously. The ESO can obtain high accuracy

observation of unmeasurable velocity state and thus offer the reliable and necessary information to the robust finite-time control law.

The main contributions and critical features of the designed control method are summarized as follows:

(1) A BNFTSMC scheme is designed to achieve singularity avoidance, high robustness, good tracking accuracy, high response speed, and finite-time convergence, which combines the merits of backstepping technique and NFTSM surface

(2) An auxiliary system based on anti-windup compensator, producing a number of signals to compensate for the negative effect of the actuator saturation, is constructed

(3) A third-order ESO is adopted to estimate the velocity state variables and external disturbances, which works as an online approximator to give the online estimated data to the BNFTSMC controller for designing the control input

(4) The designed observer-based robust finite-time control method not only can guarantee all the state tracking errors will be stabilized to equilibrium point with input saturation but also can reduce the chattering effect effectively without sacrificing robustness property

The remainder of the paper is organized as follows. Section 2 describes the preliminaries and problem formulation. Section 3 presents the formulation of the observer-based robust finite-time controller to be used in the trajectory tracking of the stratospheric satellite. Section 4 presents the results of simulations to illustrate the effectiveness of the designed control method. Finally, Section 5 concludes the paper.

2. Problem Formulation and Preliminaries

2.1. Preliminaries

2.1.1. Notations. The following notations are employed throughout this paper. $\lambda_{\max}(\cdot)$ represents the maximum element of a vector or the maximum eigenvalue of a matrix. $\lambda_{\min}(\cdot)$ represents the minimum element of a vector or the minimum eigenvalue of a matrix. $|\cdot|$ represents the absolute value of a scalar or the absolute value of each component of a vector. $\|\cdot\|$ denotes the two norm of a vector or the Frobenius norm of a matrix. For $q \in R$, the signum function $\text{sgn}(q)$ is expressed as

$$\text{sgn}(q) = \begin{cases} 1, & q > 0, \\ 0, & q = 0, \\ -1, & q < 0. \end{cases} \tag{1}$$

Meanwhile, for $q \in R$, $\text{sgn}^r(q)$ is denoted as $\text{sgn}^r(q) = |q|^r \text{sgn}(q)$. Similarly, for $\mathbf{q} = [q_1, q_2, \cdots, q_n]^T \in R^n$, $\text{sgn}^r(\mathbf{q})$ is denoted as $\text{sgn}^r(\mathbf{q}) = [|q_1|^r \text{sgn}(q_1), \cdots, |q_n|^r \text{sgn}(q_n)]^T$. For $\mathbf{q} \in R^n$, $q_i (i = 1, 2, \cdots, n)$ represents the ith component of q. Moreover, $\mathbf{I}_{n\times n}$ and $\mathbf{O}_{n\times n}$ respectively represent a $n \times n$ identity matrix and a $n \times n$ null matrix.

2.1.2. Definitions and Lemmas

Definition 1. For $q \in R$, a saturation function is defined as follows.

$$\text{sat}(q) \begin{cases} q_{\max}, & q > q_{\max}, \\ q, & q_{\min} > q > q_{\max}, \\ q_{\min}, & q < q_{\min}, \end{cases} \tag{2}$$

where $q_{\max}$ and $q_{\min}$respectively are the upper bound and lower bound of $\text{sat}(q)$. For $\mathbf{q} \in R^n$, $\text{sat}(\mathbf{q})$ is expressed as $\text{sat}(\mathbf{q}) = [\text{sat}(q_1), \text{sat}(q_2), \cdots, \text{sat}(q_n)]^T$.

Definition 2. Consider the following general dynamic system.

$$\dot{\mathbf{q}}(t) = \mathbf{f}(\mathbf{q}(t)), \ \mathbf{q}(0) = 0, \tag{3}$$

where $\mathbf{q} \in R^n$, $\mathbf{f} : D_0 \longrightarrow R^n$ is continuous and differentiable on an open neighborhood D_0 of the origin.

Lemma 3 (see [39]). *Consider the above system (3). Assume that there exist a Lyapunov function V and continuous $\mathcal{K}_\infty$ type functions $\hbar_1$ and $\hbar_2$, which satisfies the following term:*

$$\begin{aligned} &\hbar_1(\mathbf{q}) \le V(\mathbf{q}) \le \hbar_2(\mathbf{q}), \\ &\frac{dV(\mathbf{q}(t))}{dt} \le -W(\mathbf{q}(t)), \forall \|\mathbf{q}\| \ge \sigma > 0, \end{aligned} \tag{4}$$

where $W(\mathbf{q}(t))$ is a radially unbounded continuous differentiable positive definite function and σ is a finite positive constant.

Lemma 4 (see [40]). *Consider the system (3) and suppose that there exists a Lyapunov function $V(\mathbf{q})$, which holds the following inequation.*

$$V(\mathbf{q}) + \lambda V^r(\mathbf{q}) \le 0, \tag{5}$$

where $\lambda > 0$, $0 < r < 1$. Then, the finite-time stability of the system state $\mathbf{q}(t)$ are guaranteed, and the convergence time reaching the equilibrium satisfies

$$T \le \frac{V^{1-r}(\mathbf{q}_0)}{\lambda(1-\alpha)}, \tag{6}$$

where $V(\mathbf{q}_0)$ denotes the initial value of $V(\mathbf{q})$.

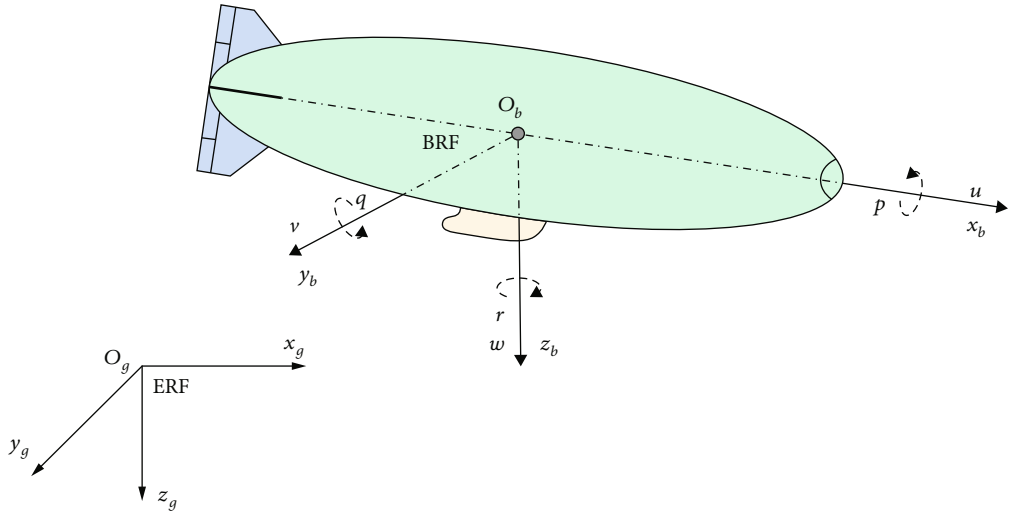

Figure 1: Structure of the stratospheric satellite.

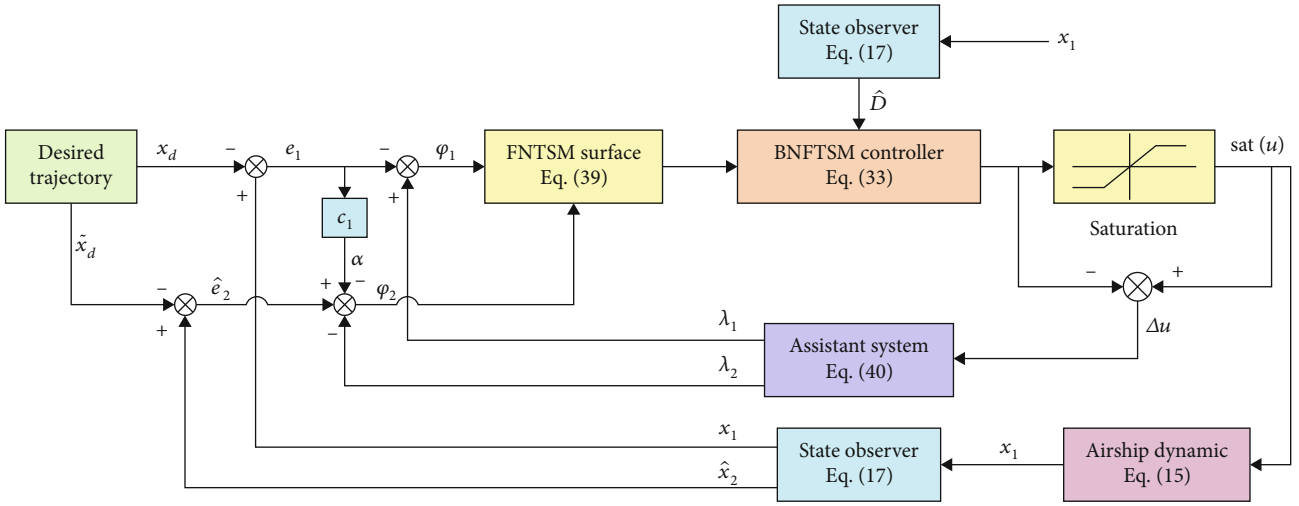

Figure 2: Block diagram of the robust finite-time controller.

Lemma 5. *For $q_i \in R$ $(i = 1, 2, \cdots, n)$ and $0 < \gamma < 1$, the following inequation holds.*

$$|q_1|^\gamma + |q_2|^\gamma + \cdots + |q_n|^\gamma \geq (|q_1| + |q_2| + \cdots + |q_n|)^\gamma. \quad (7)$$

2.2. Dynamic Model. The studied stratospheric satellite modeled as an axially symmetric rigid body, is shown in Figure 1. Before developing the stratospheric satellite dynamics, two coordinate frames are adopted to describe the motion of the stratospheric satellite, i.e., earth reference frame (ERF) and body reference frame (BRF). Then, the kinematic model is described as [16, 41]

$$\begin{bmatrix} \dot{\boldsymbol{\zeta}} \\ \dot{\boldsymbol{\gamma}} \end{bmatrix} = \mathbf{R} \begin{bmatrix} \boldsymbol{\upsilon} \\ \boldsymbol{\omega} \end{bmatrix}, \quad (8)$$

with

$$\mathbf{R} = \begin{bmatrix} \mathbf{R}_1 & \mathbf{0}_{3\times3} \\ \mathbf{0}_{3\times3} & \mathbf{R}_2 \end{bmatrix}, \quad (9)$$

where $\boldsymbol{\zeta} = [x, y, z]^T$ and $\boldsymbol{\gamma} = [\phi, \theta, \psi]^T$ respectively denote the position vector and attitude vector in ERF and $\boldsymbol{\upsilon} = [u, v, w]^T$ and $\boldsymbol{\omega} = [p, q, r]^T$ denote the linear and angular velocities in BRF. $\mathbf{R}_1$ and $\mathbf{R}_2$ are the direction cosine matrix and rotation matrix, respectively.

The dynamic model of the stratospheric satellite is expressed as follows [8].

$$\mathbf{M} \begin{bmatrix} \dot{\boldsymbol{\upsilon}} \\ \dot{\boldsymbol{\omega}} \end{bmatrix} = \begin{bmatrix} \mathbf{f}_k + \mathbf{f}_{GB} + \mathbf{f}_A + \mathbf{d}_\upsilon \\ \mathbf{n}_k + \mathbf{n}_{GB} + \mathbf{n}_A + \mathbf{d}_\omega \end{bmatrix} + \begin{bmatrix} \mathbf{u}_\upsilon \\ \mathbf{u}_\omega \end{bmatrix}, \quad (10)$$

where $\mathbf{M}$ is mass matrix. $\mathbf{f}_{GB}$ represents the sum of the gravity and buoyancy vector. $\mathbf{n}_{GB}$ is the corresponding torque

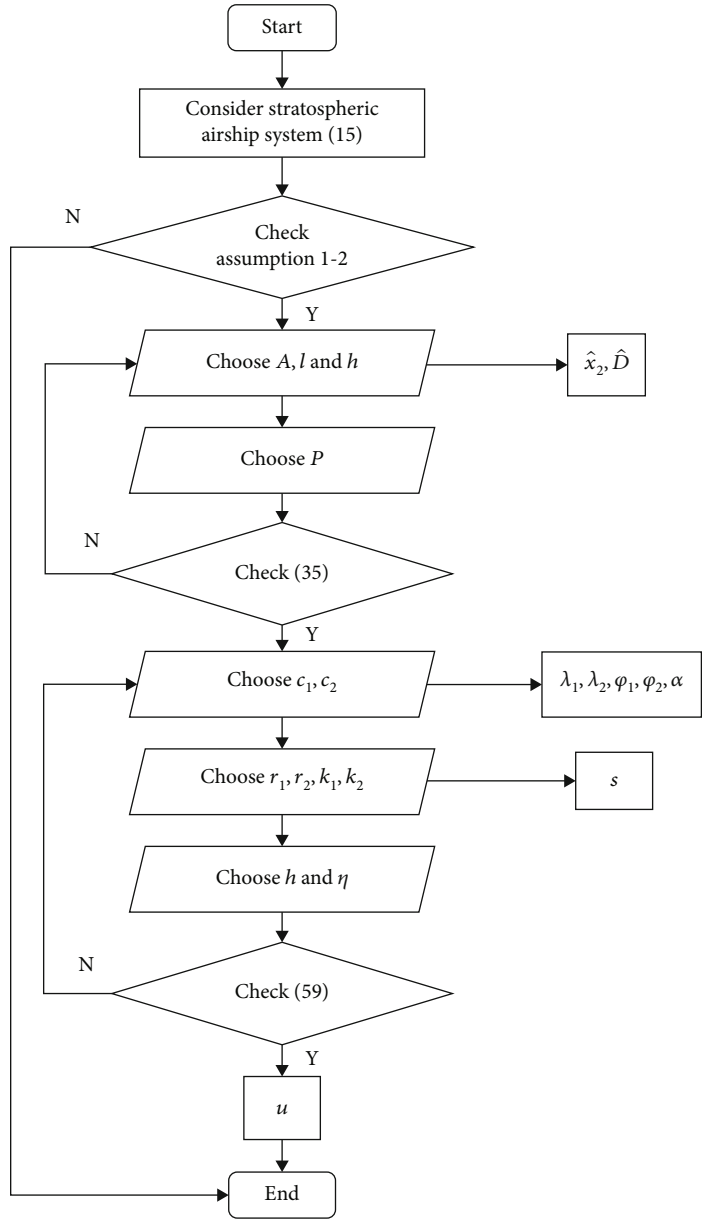

Figure 3: The flow chart of the robust finite-time controller design procedure.

generated by $\mathbf{f}_{GB}$. $\mathbf{f}_k$ and $\mathbf{n}_k$ represent the kinetics force and torque, respectively; $\mathbf{f}_A$ and $\mathbf{n}_A$ represent aerodynamic force and torque, respectively; $\mathbf{u}_v$ and $\mathbf{u}_\omega$ represent control force and torque, respectively. The details of (10) are presented in Ref. [29].

2.3. Problem Formulation. For simplicity, the dynamic model is rewritten as follows.

$$\begin{cases} \dot{\mathbf{x}}_1 = \mathbf{x}_2, \\ \dot{\mathbf{x}}_2 = \mathbf{F}(\mathbf{x}_1, \mathbf{x}_2) + \mathbf{B}(\mathbf{x}_1)\mathbf{u} + \mathbf{D}, \end{cases} \tag{11}$$

with

$$\mathbf{F} = \dot{\mathbf{R}}\mathbf{R}^{-1}\dot{\mathbf{x}} + \mathbf{R}\mathbf{M}^{-1}\begin{bmatrix} \mathbf{f}_k + \mathbf{f}_{GB} + \mathbf{f}_A \\ \mathbf{n}_k + \mathbf{n}_{GB} + \mathbf{n}_A \end{bmatrix},$$

$$\mathbf{D} = \mathbf{R}\mathbf{M}^{-1}\begin{bmatrix} \mathbf{d}_v \\ \mathbf{d}_w \end{bmatrix}, \ \mathbf{B} = \mathbf{R}\mathbf{M}^{-1}, \tag{12}$$

where $\mathbf{x}_1 = [\boldsymbol{\zeta}^T, \boldsymbol{\gamma}^T]^T$ and $\mathbf{x}_2 = [\dot{\boldsymbol{\zeta}}^T, \dot{\boldsymbol{\gamma}}^T]^T$ are the system state vectors. $\mathbf{u} = [u_1, u_2, u_3, u_4, u_5, u_6]^T$ is the control input vector. $\dot{\mathbf{R}}$ is the time derivative of $\mathbf{R}$.

Table 1: Controller parameters.

Parameter	Value	Parameter	Value
l	10	$\mathbf{r}_1$	Diag (8.7, 8.7, 8.7, 0.03, 0.03, 0.03)
h	50	$\mathbf{r}_2$	Diag (0.5, 0.5, 0.5, 0.8, 0.8, 0.8)
a_1	3	k_1	1.2
a_2	3	k_2	1.0885
a_2	0.005	$\boldsymbol{\rho}$	Diag (0.2, 0.2, 0.2, 0.2, 0.2, 0.2)
$\mathbf{c}_1$	Diag (0.2, 0.2, 0.2, 0.2, 0.2, 0.2)	$\boldsymbol{\eta}$	Diag (0.2, 0.2, 0.2, 0.2, 0.2, 0.2)
$\mathbf{c}_2$	Diag (0.2, 0.2, 0.2, 0.2, 0.2, 0.2)		

Assumption 6. The lumped external disturbances $\mathbf{D}$ and its derivative are assumed to be bounded, which satisfies

$$\begin{cases} \|\mathbf{D}\| \le \delta, \\ \|\mathbf{D}\| \le \delta_1, \end{cases} \tag{13}$$

where δ and δ_1 are finite positive constants.

Assumption 7. The smooth function $\mathbf{F}(\boldsymbol{\chi})$ is Lipschitz continuous, i.e., $\forall t \ge 0$, then $\exists L \in R^+$, satisfying the following in equation

$$|\mathbf{F}(\boldsymbol{\chi}) - \mathbf{F}(\widehat{\boldsymbol{\chi}})| = L\|\boldsymbol{\chi} - \widehat{\boldsymbol{\chi}}\|, \tag{14}$$

where $\boldsymbol{\chi} \in R^n$, $\widehat{\boldsymbol{\chi}} \in R^n$. L is Lipschitz constant.

Considering the input saturation constraint of the actuator, Equation (11) can be deformed as:

$$\begin{cases} \dot{\mathbf{x}}_1 = \mathbf{x}_2, \\ \dot{\mathbf{x}}_2 = \mathbf{F} + \mathbf{B}\mathrm{sat}(\mathbf{u}) + \mathbf{D}. \end{cases} \tag{15}$$

The trajectory tracking control problem is intended to design an effective controller that drives the stratospheric satellite to track the desired trajectory with fast convergence rate, high accuracy, and strong robustness. More specifically, the control objective can be concretely described as follows: $\mathbf{x}_0$ and the desired state $\mathbf{x}_d$, develop the appropriate control law $\mathbf{u}$ for system (15) subject to the external disturbances and input saturation, such that the finite-time convergence of tracking errors with satisfactory tracking precision can be achieved.

3. Control Design

In this section, a novel robust finite-time controller based on BNFTSMC scheme is presented for the trajectory tracking of the stratospheric satellite subject to time-varying disturbance and input saturation. A third-order ESO is designed to estimate the velocity state and time-varying disturbance. On the basis of the anti-windup compensator, an auxiliary system is constructed to compensate for the saturation difference directly. Finally, based on the measurability of the system output and the estimations of the system velocity state and external disturbance, the BNFTSMC strategy with the auxiliary system is developed for designing the trajectory tracking controller. The designed flight control scheme for trajectory tracking of a stratospheric satellite is illustrated in Figure 2.

3.1. ESO Design. In general, the output of the stratospheric satellite system can be directly measured by sensors, while the other state variables are difficult to obtain directly. For dealing with the problem caused by the unmeasurable states, an extended state observer (ESO) is proposed, where $\mathbf{x}_2$ and $\mathbf{D}$ are regarded as extended states. $\mathbf{x}_2$ is online estimated by the designed ESO and used for providing velocity information for the controller design. $\widehat{\mathbf{D}}$ is the estimated value of $\mathbf{D}$, and is used to compensate for the effect of system, improving the robustness and adaptability of the closed-loop system.

Define $\mathbf{z}_1 = \mathbf{x}_1$, $\mathbf{z}_2 = \mathbf{x}_2/l\mathbf{z}_3 = \boldsymbol{D}/l^2$. By differentiating the state variables $\mathbf{z}_1$, $\mathbf{z}_2$, and $\mathbf{z}_3$, the stratospheric satellite system given by Equation (15) can be rewritten as a third-order equation of system states.

$$\begin{cases} \dot{\mathbf{z}}_1 = l\mathbf{z}_2, \\ \dot{\mathbf{z}}_2 = \dfrac{1}{l}\mathbf{F}(\mathbf{z}_1, \mathbf{z}_2) + \dfrac{1}{l}\mathbf{B}(\mathbf{z}_1)\mathrm{sat}(\mathbf{u}) + l\mathbf{z}_3, \\ \dot{\mathbf{z}}_3 = \dot{\mathbf{D}}, \end{cases} \tag{16}$$

where l is the designed scaling gain.

Let $\widehat{\mathbf{z}}_1$, $\widehat{\mathbf{z}}_2$, and $\widehat{\mathbf{z}}_3$ denote the estimated values of $\mathbf{z}_1$, $\mathbf{z}_2$, and $\mathbf{z}_3$, respectively. Then, the observation errors are defined as $\tilde{\mathbf{z}}_1 = \widehat{\mathbf{z}}_1 - \mathbf{z}_1$, $\tilde{\mathbf{z}}_2 = \widehat{\mathbf{z}}_2 - \mathbf{z}_2$, and $\tilde{\mathbf{z}}_3 = \widehat{\mathbf{z}}_3 - \mathbf{z}_3$. Then, for the stratospheric satellite system (15), a third-order ESO is constructed as

$$\begin{cases} \tilde{\mathbf{z}}_1 = \mathbf{z}_1 - \widehat{\mathbf{z}}_1, \\ \dot{\widehat{\mathbf{z}}}_1 = l\widehat{\mathbf{z}}_2 + a_1 h l\tilde{\mathbf{z}}_1, \\ \dot{\widehat{\mathbf{z}}}_2 = \dfrac{1}{l}\mathbf{F}(\mathbf{z}_1, \widehat{\mathbf{z}}_2) + \dfrac{1}{l}\mathbf{B}(\mathbf{z}_1)\mathrm{sat}(\mathbf{u}) + l\widehat{\mathbf{z}}_3 + a_2 h^2 l\tilde{\mathbf{z}}_1, \\ \dot{\widehat{\mathbf{z}}}_3 = a_3 h^3 l\tilde{\mathbf{z}}_1, \end{cases} \tag{17}$$

where h is a gain constant, which satisfies $h > l$. a_1, a_2, and a_3 are positive constants, which satisfy the following

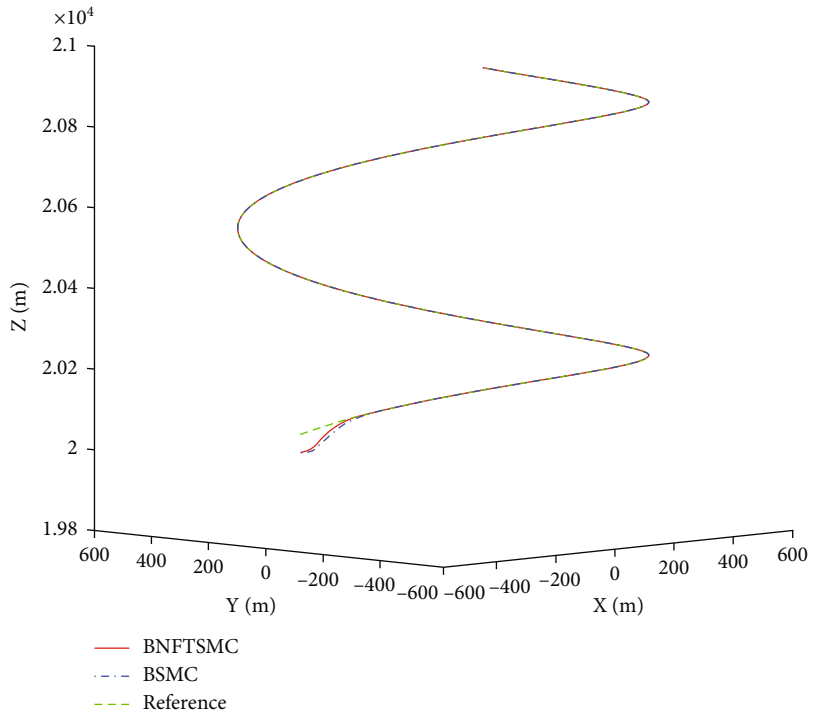

Figure 4: Trajectory tracking results in three-dimensional space.

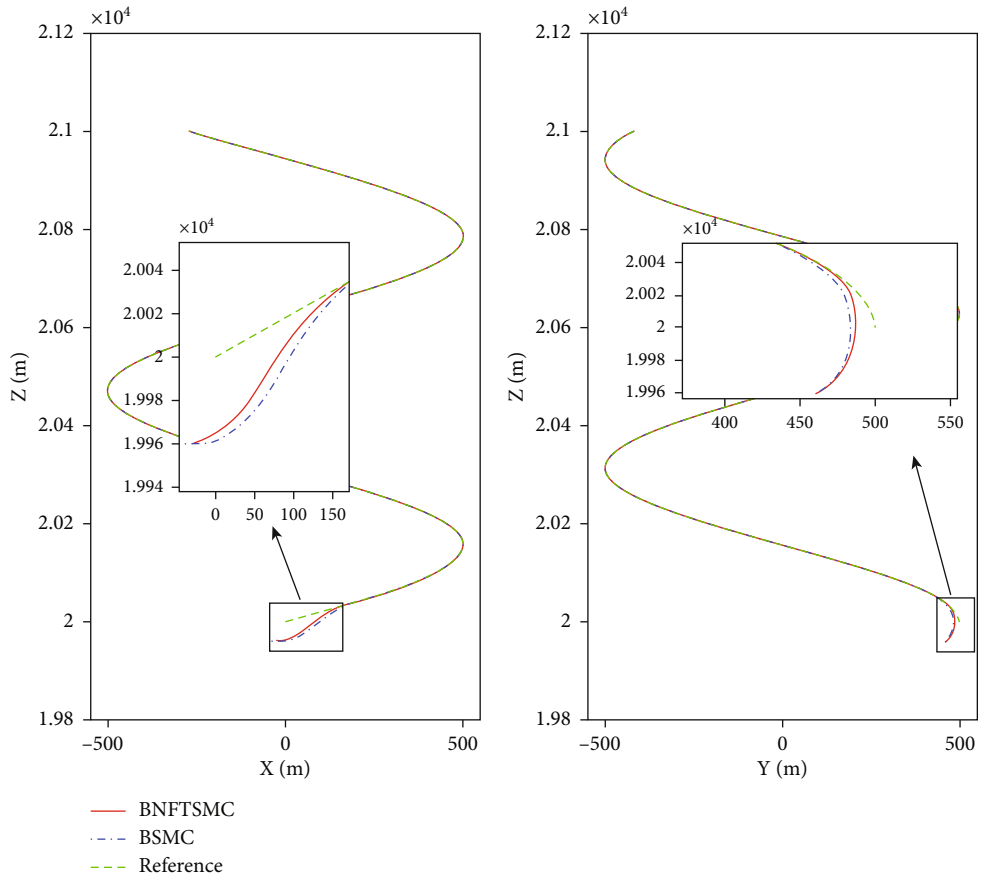

Figure 5: Projection of the trajectory tracking results on x-z plane and y-z plane.

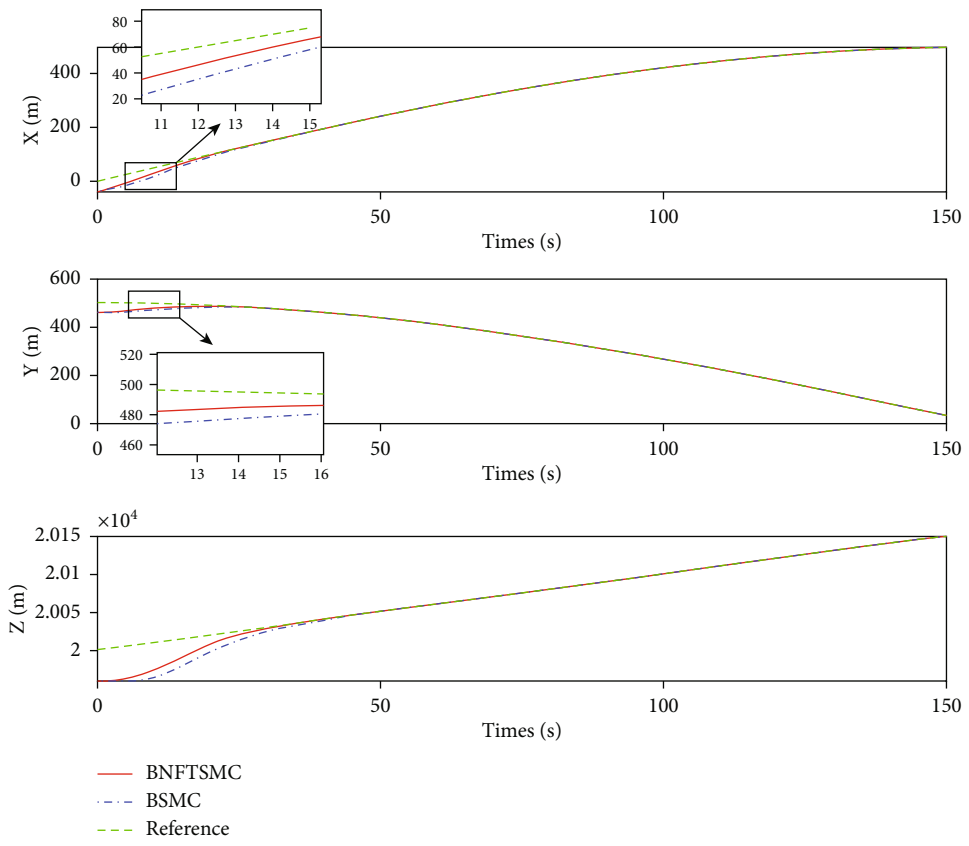

Figure 6: Position tracking responses.

Hurwitz matrix:

$$\boldsymbol{A} = \begin{bmatrix} -a_1 & 1 & 0 \\ -a_2 & 0 & 1 \\ -a_3 & 0 & 0 \end{bmatrix} \tag{18}$$

Comparing Equations (16) and (17), the error differential system of the ESO is derived.

$$\begin{cases} \dot{\tilde{\mathbf{z}}}_1 = -a_1 hl\tilde{\mathbf{z}}_1 + l\tilde{\mathbf{z}}_2, \\ \dot{\tilde{\mathbf{z}}}_2 = -a_2 h^2 l\tilde{\mathbf{z}}_1 + l\tilde{\mathbf{z}}_3 + \dfrac{1}{l}(\mathbf{F}(\mathbf{z}_1, \mathbf{z}_2) - \mathbf{F}(\mathbf{z}_1, \hat{\mathbf{z}}_2)), \\ \dot{\tilde{\mathbf{z}}}_3 = -a_3 h^3 l\tilde{\mathbf{z}}_1 + \dot{\boldsymbol{D}} \end{cases} \tag{19}$$

In order to facilitate the stability analysis, the error differential system in scalar form can be obtained as

$$\begin{cases} \dot{\tilde{z}}_{1i} = -a_1 hl\tilde{z}_{1i} + l\tilde{z}_{2i}, \\ \dot{\tilde{z}}_{2i} = -a_2 h^2 l\tilde{z}_{1i} + l\tilde{z}_{3i} + \dfrac{1}{l}(F_i(\mathbf{z}_1, \mathbf{z}_2) - F_i(\mathbf{z}_1, \hat{\mathbf{z}}_2)), \\ \dot{\tilde{z}}_{3i} = -a_3 h^3 l\tilde{z}_{1i} + \dot{D}_i(t). \end{cases} \tag{20}$$

Let us introduce $\dot{\varepsilon}_j = h^{3-i}\tilde{z}_j (j = 1, 2, 3)$. The above system can be transformed as

$$\begin{cases} \dot{\varepsilon}_1 = lh(\varepsilon_2 - a_1\varepsilon_1), \\ \dot{\varepsilon}_2 = lh(\varepsilon_3 - a_2\varepsilon_1) + \dfrac{h}{l}(F_i(\mathbf{z}_1, \mathbf{z}_2) - F_i(\mathbf{z}_1, \hat{\mathbf{z}}_2)), \\ \dot{\varepsilon}_3 = -lha_3\varepsilon_1 + \dot{D}_i(t). \end{cases} \tag{21}$$

Let $\boldsymbol{\varepsilon} = [\varepsilon_1, \varepsilon_2, \varepsilon_3]^T$, $\tilde{\mathbf{F}} = [0, F_i(z_1, z_2) - F_i(z_1, \hat{z}_2), 0]^T$, and $\mathbf{f} = [0, 0, \dot{D}_i]^T$, then Equation (21) can be rewritten as

$$\dot{\boldsymbol{\varepsilon}} = lh\mathbf{A}\boldsymbol{\varepsilon} + \frac{h}{l}\tilde{\mathbf{F}} + \mathbf{f}. \tag{22}$$

Since A is a Hurwitz matrix, the following Lyapunov equation can be satisfied.

$$\mathbf{A}^{\mathrm{T}}\mathbf{P} + \mathbf{P}\mathbf{A} = -\mathbf{I}_{3\times 3}. \tag{23}$$

Theorem 8. *For the stratospheric satellite system in the presence of dynamic uncertainty, if the ESO is designed as Equation (17), the ESO is uniformly ultimately bounded, and the observation error* $\mathbf{z}_e = [\tilde{z}_{1i}, \tilde{z}_{2i}, \tilde{z}_{3i}]^T$ *will converge to a small neighborhood of origin.*

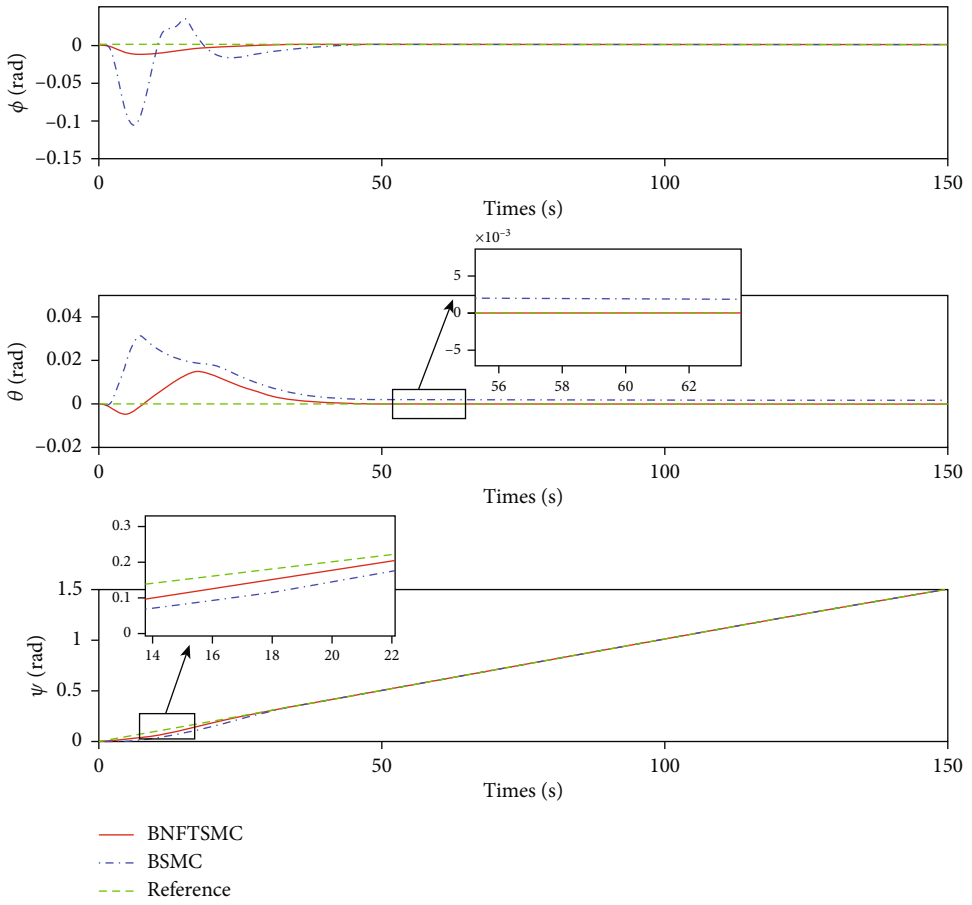

Figure 7: Attitude tracking responses.

Proof. Define the Lyapunov function as follows.

$$V_1 = \boldsymbol{\varepsilon}^T \mathbf{P} \boldsymbol{\varepsilon}. \tag{24}$$

□

Differentiating Equation (24) with respect to time yields

$$\dot{V}_1 = \dot{\boldsymbol{\varepsilon}}^T \mathbf{P} \boldsymbol{\varepsilon} + \boldsymbol{\varepsilon}^T \mathbf{P} \dot{\boldsymbol{\varepsilon}}. \tag{25}$$

Substituting Equation (22) into Equation (25), it follows

$$\begin{aligned} \dot{V}_1 &= lh\left(\mathbf{A}\mathbf{P} + \mathbf{P}\mathbf{A}^T\right)^T \boldsymbol{\varepsilon}^T \boldsymbol{\varepsilon} + 2\frac{h}{l}\boldsymbol{\varepsilon}^T \mathbf{P}\tilde{\mathbf{F}} + 2\boldsymbol{\varepsilon}^T \mathbf{P}\mathbf{f} \\ &= -lh\boldsymbol{\varepsilon}^T \boldsymbol{\varepsilon} + 2\frac{h}{l}\boldsymbol{\varepsilon}^T \mathbf{P}\tilde{\mathbf{F}} + 2\boldsymbol{\varepsilon}^T \mathbf{P}\mathbf{f}. \end{aligned} \tag{26}$$

Based on Lemma 3, it is clearly known that

$$\lambda_{\min}(\mathbf{P})\|\boldsymbol{\varepsilon}\|^2 \le V_1 \le \lambda_{\max}(\mathbf{P})\|\boldsymbol{\varepsilon}\|^2. \tag{27}$$

According to Assumption 7 and $\dot{\varepsilon}_j = h^{3-i}\tilde{z}_j$, $(j = 1, 2, 3)$, we have

$$\begin{aligned} \left\|\tilde{\mathbf{F}}\right\| &= \left|F_i(z_1, z_2) - F_i(z_1, \hat{z}_2)\right| \\ &= L\left\|\left[z_1 - z_1, z_2 - \hat{z}_2\right]^T\right\| \\ &= L\left\|\left[0, \frac{\varepsilon_2}{h}\right]^T\right\| \\ &\le L\frac{\|\varepsilon_2\|}{h}. \end{aligned} \tag{28}$$

Referring to Assumption 6 and $\mathbf{z}_3 = \mathbf{D}/l^2$, we can get

$$\|\mathbf{f}\| = \left|\dot{D}_i(t)\right| \le \frac{\delta_1}{l^2}. \tag{29}$$

Based on Equation (27) and Equation (28), we can get that

$$\boldsymbol{\varepsilon}^T \mathbf{P}\tilde{\mathbf{F}} \le \left\|\boldsymbol{\varepsilon}^T \mathbf{P}\tilde{\mathbf{F}}\right\| \le \left\|\boldsymbol{\varepsilon}^T\right\|\|\mathbf{P}\|\left\|\tilde{\mathbf{F}}\right\| \le \frac{L\lambda_{\max}(\mathbf{P})\left\|\boldsymbol{\varepsilon}^2\right\|}{h}. \tag{30}$$

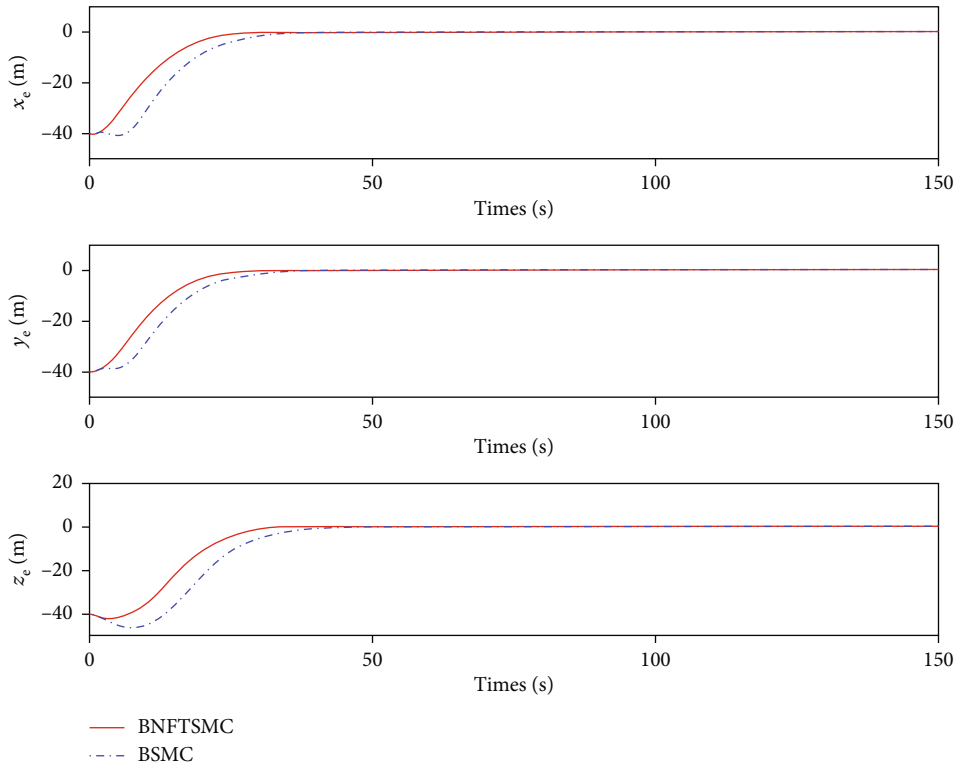

Figure 8: Position tracking errors.

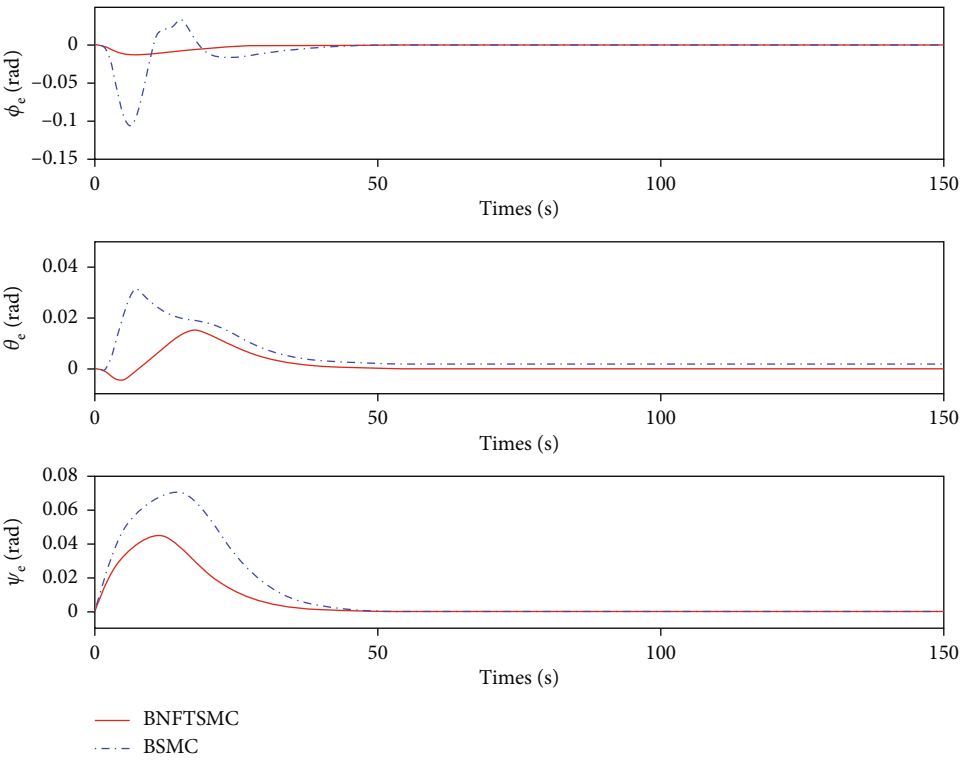

Figure 9: Attitude tracking errors.

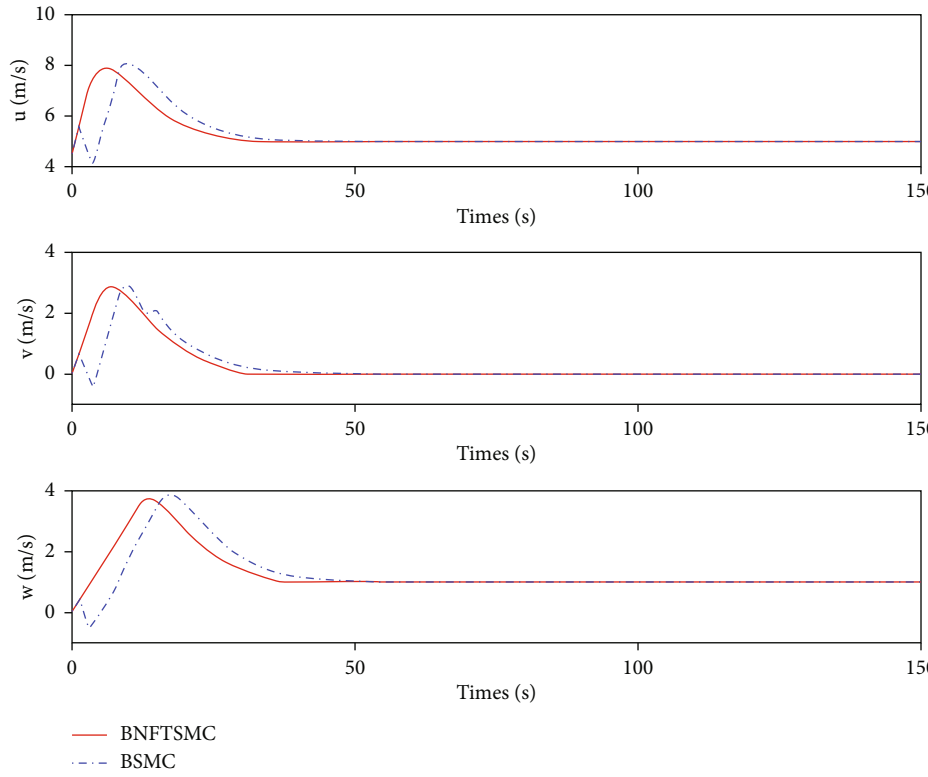

Figure 10: Linear velocity tracking responses.

According to Equation (27) and Equation (29), we have

$$\boldsymbol{\varepsilon}^T\mathbf{P}\mathbf{f} \le \left\|\boldsymbol{\varepsilon}^T\mathbf{P}\mathbf{f}\right\| \le \left\|\boldsymbol{\varepsilon}^T\right\|\|\mathbf{P}\|\|\mathbf{f}\| \le \frac{\delta_1\lambda_{\max}(\mathbf{P})\left\|\boldsymbol{\varepsilon}^2\right\|}{l^2}. \tag{31}$$

Substituting Equation (30) and Equation (31) into Equation (26), we can conclude that

$$\begin{aligned}\dot{V}_1 &\le -lh\|\boldsymbol{\varepsilon}\|^2 + \frac{2L\lambda_{\max}(\mathbf{P})\|\boldsymbol{\varepsilon}\|^2}{l} + \frac{2\delta_1\lambda_{\max}(\mathbf{P})\|\boldsymbol{\varepsilon}\|}{l^2} \\ &= -\left(lh - \frac{2L\lambda_{\max}(\mathbf{P})}{l}\right)\|\boldsymbol{\varepsilon}\|^2 + \frac{2\delta_1\lambda_{\max}(\mathbf{P})\|\boldsymbol{\varepsilon}\|}{l^2} \\ &= -(1-\ell)\left(lh - \frac{2L\lambda_{\max}(\mathbf{P})}{l}\right)\|\boldsymbol{\varepsilon}\|^2 - \bar{\lambda}(\boldsymbol{\varepsilon})\|\boldsymbol{\varepsilon}\|,\end{aligned} \tag{32}$$

where $\bar{\lambda}(\boldsymbol{\varepsilon}) = \ell(lh - (2L\lambda_{\max}(\mathbf{P})/l))\|\boldsymbol{\varepsilon}\| - (2\delta_1\lambda_{\max}(\mathbf{P})\|\boldsymbol{\varepsilon}\|/l^2)$, $0 < \ell < 1$. By selecting the proper value of l, the system stability can be guaranteed. For that purpose, assume that $\bar{\lambda}(\boldsymbol{\varepsilon}) \ge 0$, then the following inequation can be obtained.

$$\ell\left(lh - \frac{2L\lambda_{\max}(\mathbf{P})}{l}\right)\|\boldsymbol{\varepsilon}\| > \frac{2\delta\lambda_{\max}(\mathbf{P})\|\boldsymbol{\varepsilon}\|}{l^2} > 0. \tag{33}$$

Then, by defining $\Upsilon = 2\delta_1\lambda_{\max}(\mathbf{P})/\ell l[l^2\gamma - 2L\lambda_{\max}(\mathbf{P})]$, we can obtain that

$$\begin{cases} l > \sqrt{\dfrac{2L\lambda_{\max}(\mathbf{P})}{h}}, \\ \|\boldsymbol{\varepsilon}\| \ge \Upsilon > 0. \end{cases} \tag{34}$$

Thus, as long as l satisfies the above inequation, $\bar{\lambda}(\boldsymbol{\varepsilon}) > 0$ can be ensured. Then, set $H(\boldsymbol{\varepsilon}) = (1-\ell)(lh - (2L\lambda_{\max}(\mathbf{P})/l))\|\boldsymbol{\varepsilon}\|^2 + \bar{\lambda}(\boldsymbol{\varepsilon})\|\boldsymbol{\varepsilon}\|$, and (32) can be transformed into

$$\dot{V}_1(\boldsymbol{\varepsilon}) < -H(\boldsymbol{\varepsilon}) < 0. \tag{35}$$

Thus, let $\hbar_1(\|\boldsymbol{\varepsilon}\|) = \lambda_{\min}(\mathbf{P})\|\boldsymbol{\varepsilon}\|^2$ and $\hbar_2(\|\boldsymbol{\varepsilon}\|) = \lambda_{\max}(\mathbf{P})\|\boldsymbol{\varepsilon}\|^2$. Based on the above analysis, we can get

$$\|z\| \le \|\boldsymbol{\varepsilon}\| \le \hbar_1^{-1}(\hbar_2(\Upsilon)) = \Upsilon\sqrt{\frac{\lambda_{\max}(\mathbf{P})}{\lambda_{\min}(\mathbf{P})}}. \tag{36}$$

So, the extended state observer is progressively stable, and the observation error $\tilde{\mathbf{z}} = [\tilde{z}_1, \tilde{z}_2, \tilde{z}_3]^T$ is bounded and can converge to the set range.

3.2. BNFTSMC Design. In this section, inspired by Ref. [24] and Ref. [42], a robust finite-time controller based on the backstepping technique and NFTSMC method is further developed. The proposed BNFTSMC strategy combines the merits of backstepping technique and NFTSMC method. Then, an auxiliary system is added to the BNFTSMC design to cope with the saturation problem and achieve favorable

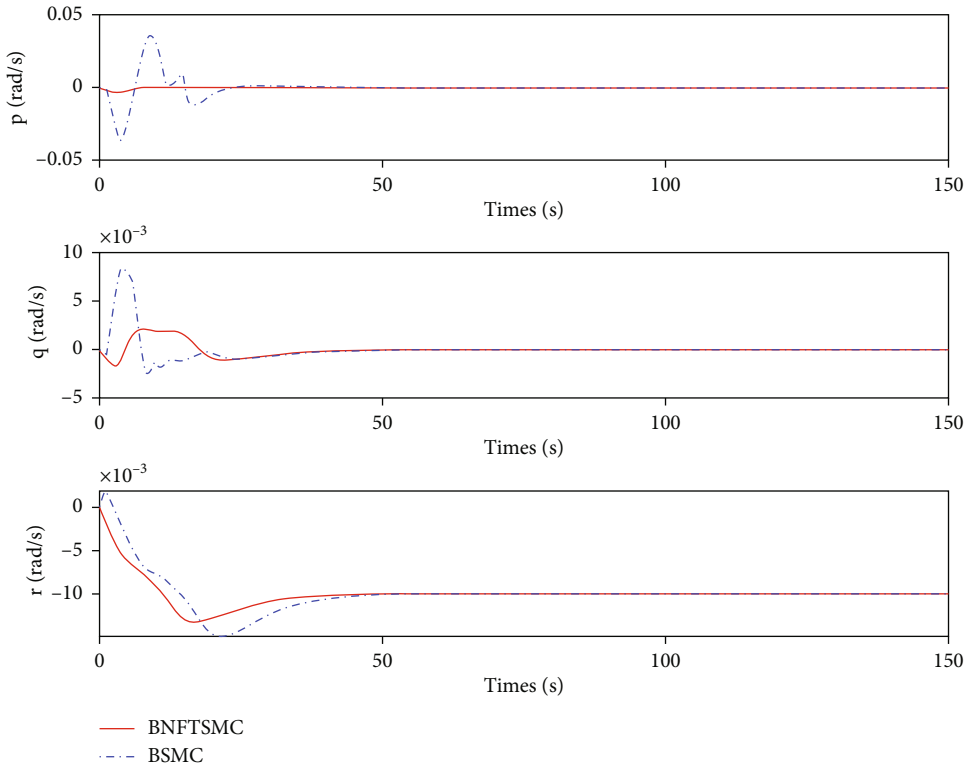

Figure 11: Angular velocity tracking responses.

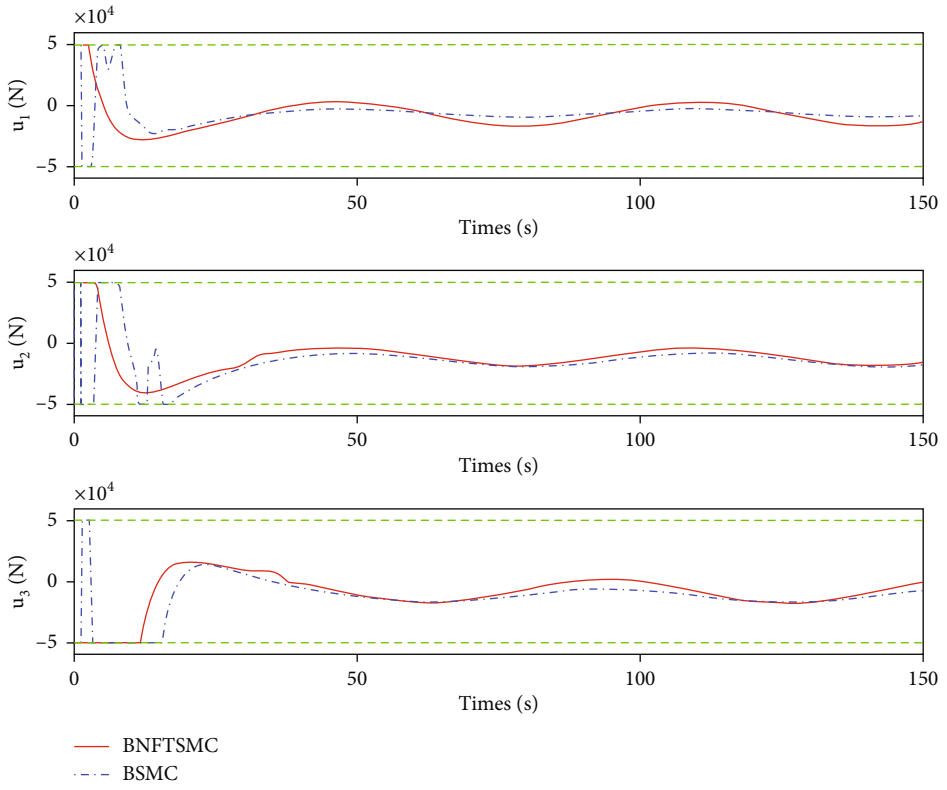

Figure 12: Force inputs.

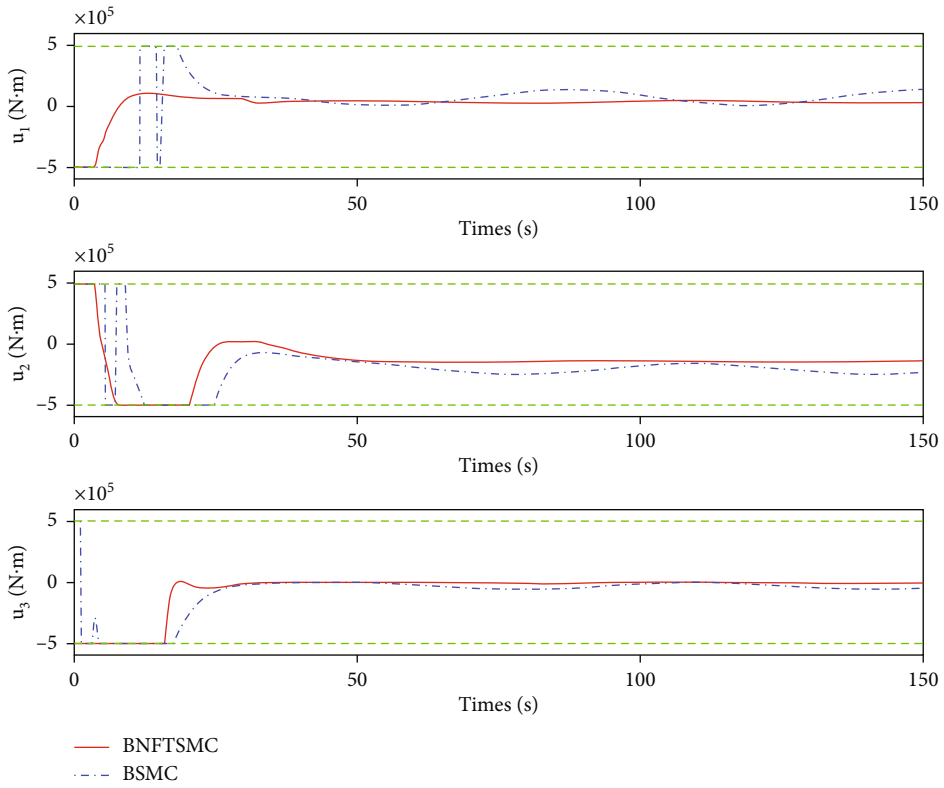

Figure 13: Torque inputs.

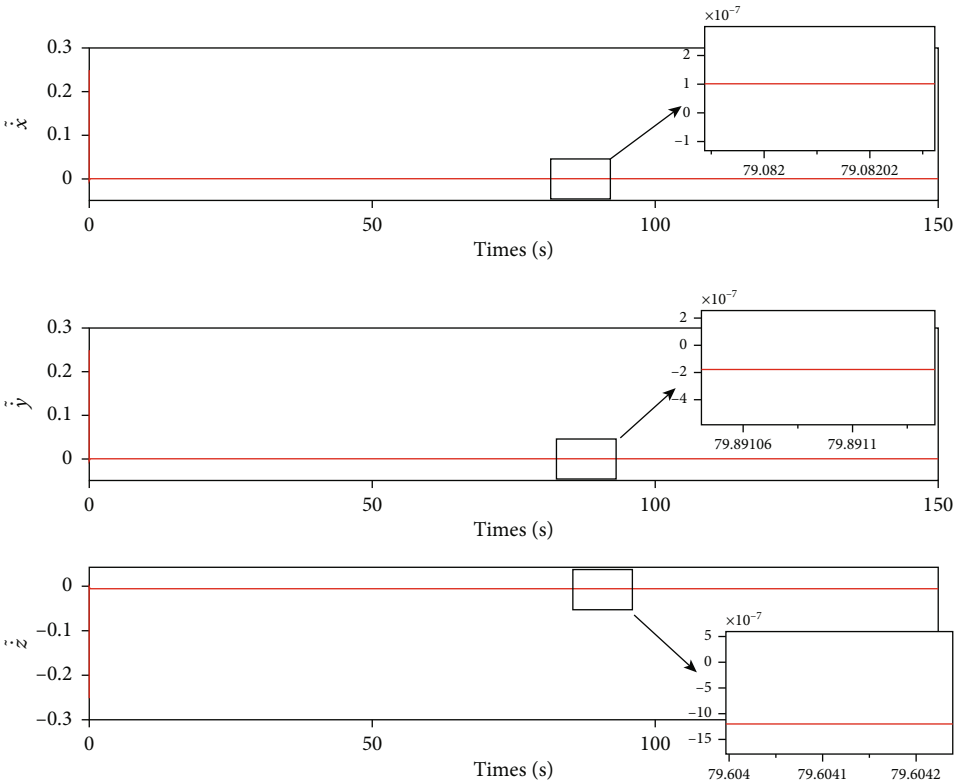

Figure 14: Observation errors of ESO in position subsystem.

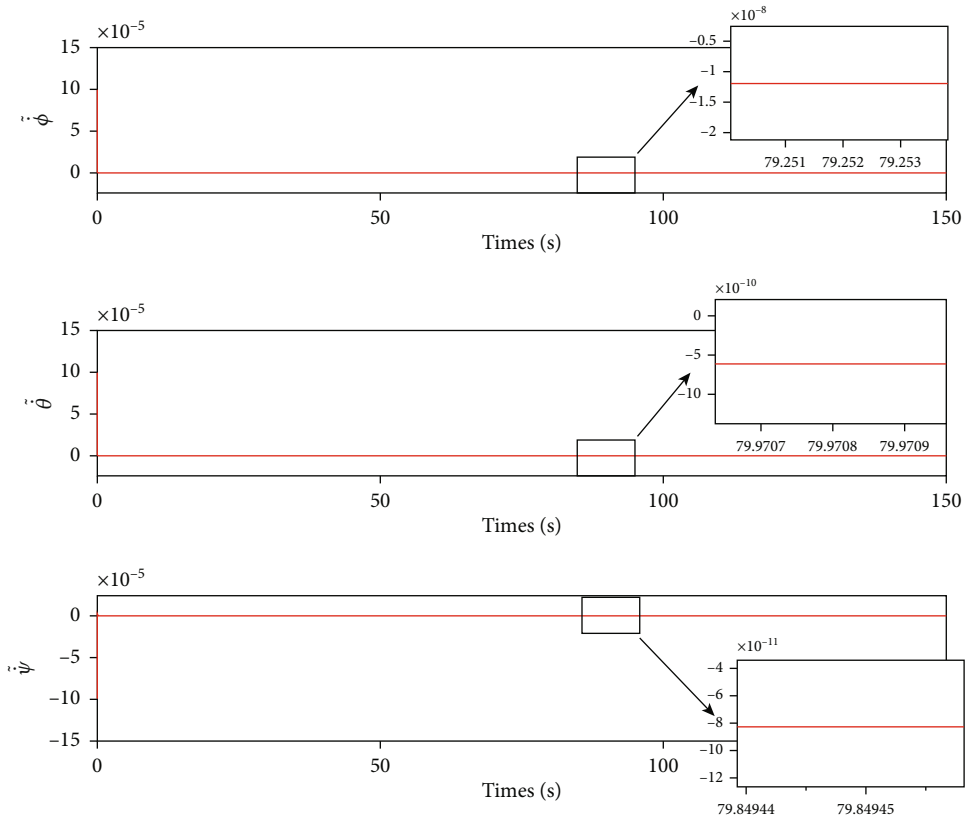

Figure 15: Observation errors of ESO in attitude subsystem.

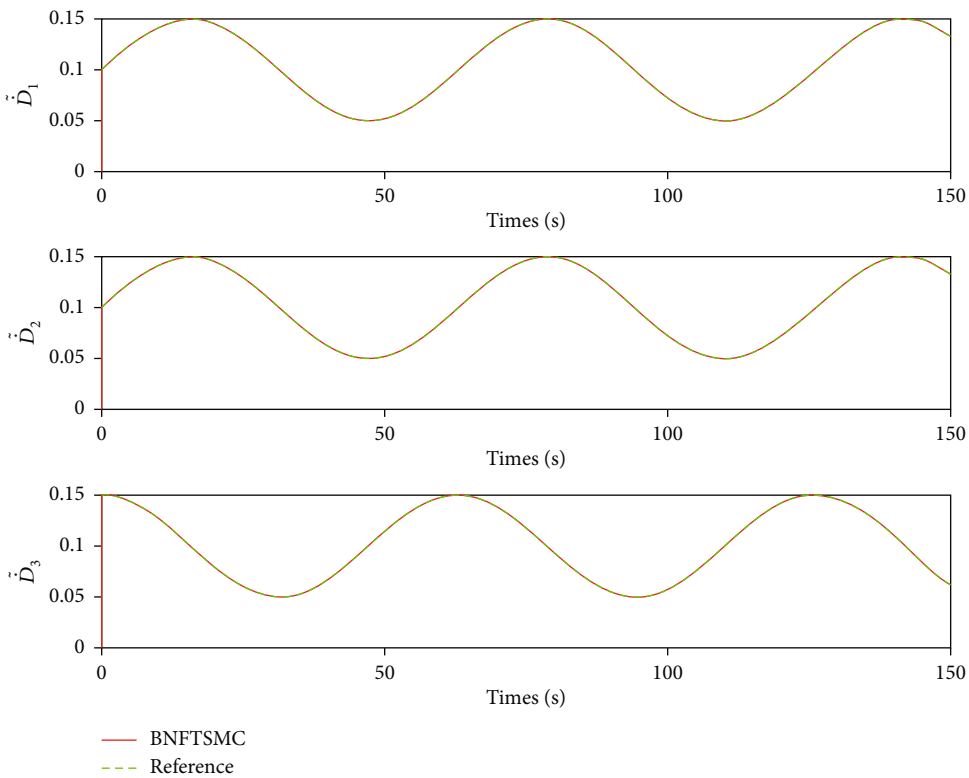

Figure 16: Estimation of the disturbances in position subsystem.

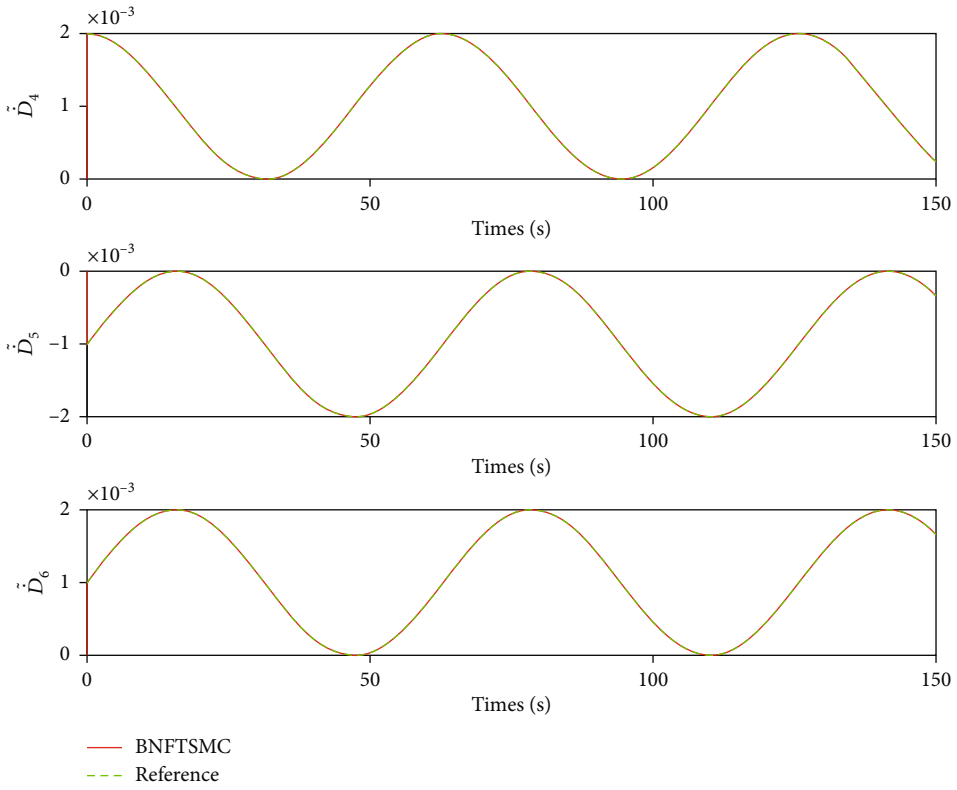

Figure 17: Estimation of the disturbances in position subsystem.

control performance. Moreover, the linear and angular velocity and external disturbance deriving from the proposed ESO are provided to construct the BNFTSMC control law, which alleviates the chattering effectively.

The tracking error dynamics of the stratospheric satellite system are obtained as follows.

$$\begin{aligned} \mathbf{e}_1 &= \mathbf{x}_1 - \mathbf{x}_d, \\ \mathbf{e}_2 &= \mathbf{x}_2 - \dot{\mathbf{x}}_d. \end{aligned} \tag{37}$$

Considering the observation results of the proposed ESO, the estimated value of $\mathbf{e}_2$ can be written as

$$\hat{\mathbf{e}}_2 = \hat{\mathbf{x}}_2 - \dot{\mathbf{x}}_d. \tag{38}$$

A NFTSM surface is selected as follows:

$$\mathbf{s} = \mathbf{e}_1 + \mathbf{r}_1 \operatorname{sgn}^{k_1}(\mathbf{e}_1) + \mathbf{r}_2 \operatorname{sgn}^{k_2}(\hat{\mathbf{e}}_2), \tag{39}$$

where $\mathbf{r}_1$ and $\mathbf{r}_2$ are designed positive definite diagonal matrices and k_1 and k_2 are positive numbers which satisfy $k_1 \geq k_2$ and $1 < k_2 < 2$.

Remark 9 (see [39]). Utilizing the above sliding surface, when the system states are far from the equilibrium states, $\mathbf{r}_1 \operatorname{sgn}^{k_1}(\mathbf{e}_1)$ has a dominant position and ensure a high convergence rate, compared with $\mathbf{r}_2 \operatorname{sgn}^{k_2}(\hat{\mathbf{e}}_2)$; when the system states approach the equilibrium states, $\mathbf{r}_2 \operatorname{sgn}^{k_2}(\hat{\mathbf{e}}_2)$ guarantees finite-time convergence.

To attenuate the negative effect of input saturation affecting the satellite dynamics, an auxiliary system is introduced to compensate for the saturation problem, which is constructed as:

$$\begin{cases} \dot{\boldsymbol{\lambda}}_1 = -\mathbf{c}_1\boldsymbol{\lambda}_1 + \boldsymbol{\lambda}_2, \\ \dot{\boldsymbol{\lambda}}_2 = -\mathbf{c}_2\boldsymbol{\lambda}_2 + \mathbf{B}\Delta\mathbf{u}, \end{cases} \tag{40}$$

where $\Delta\mathbf{u} = \operatorname{sat}(\mathbf{u}) - \mathbf{u}$. $\boldsymbol{\lambda}_1, \boldsymbol{\lambda}_2 \in R^6$ are the state variables of the auxiliary system. $\mathbf{c}_1$ and $\mathbf{c}_2$ are the positive definite diagonal matrices to be designed.

Based on the backstepping method, the following change of coordinates is introduced.

$$\begin{cases} \boldsymbol{\varphi}_1 = \boldsymbol{e}_1 - \boldsymbol{\lambda}_1, \\ \boldsymbol{\varphi}_2 = \hat{\boldsymbol{e}}_2 - \boldsymbol{\alpha} - \boldsymbol{\lambda}_2. \end{cases} \tag{41}$$

where the virtual control function $\boldsymbol{\alpha}$ is designed as

$$\boldsymbol{\alpha} = -\mathbf{c}_1\boldsymbol{e}_1. \tag{42}$$

Differentiating $\boldsymbol{\varphi}_1$ with respect to time, we have

$$\dot{\boldsymbol{\varphi}}_1 = \hat{\boldsymbol{e}}_2 - \dot{\boldsymbol{\lambda}}_1. \tag{43}$$

From Equations (41)–(43), we get

$$\dot{\boldsymbol{\varphi}}_1 = -\mathbf{c}_1\boldsymbol{\varphi}_1 + \boldsymbol{\varphi}_2. \tag{44}$$

A candidate Lyapunov function is defined as

$$V_2 = \frac{1}{2}\boldsymbol{\varphi}_1^T\boldsymbol{\varphi}_2. \tag{45}$$

The derivative of V_2 is derived as

$$\dot{V}_2 = \boldsymbol{\varphi}_1^T\dot{\boldsymbol{\varphi}}_1 = -\boldsymbol{\varphi}_1^T\mathbf{c}_1\boldsymbol{\varphi}_1 + \boldsymbol{\varphi}_1^T\boldsymbol{\varphi}_2. \tag{46}$$

Remark 10. We can see that, once term $\boldsymbol{\varphi}_1^T\boldsymbol{\varphi}_2$ is eliminated in the following design, $\dot{V}_2 = -\boldsymbol{\varphi}_1^T\mathbf{c}_1\boldsymbol{\varphi}_1 < 0$ can be obtained, and the states $\boldsymbol{\varphi}_1$ and $\boldsymbol{\varphi}_2$ will be asymptotically stable.

Next, differentiating $\boldsymbol{\varphi}_2$ with respect to time, yields

$$\begin{aligned}\dot{\boldsymbol{\varphi}}_2 &= \hat{\boldsymbol{e}}_2 - \dot{\boldsymbol{\alpha}} - \dot{\boldsymbol{\lambda}}_2 \\ &= \mathbf{F}(\mathbf{x}_1, \hat{\mathbf{x}}_2) + \mathbf{B}(\mathbf{x}_1)\mathrm{sat}(\mathbf{u}) + \hat{\mathbf{D}} - \ddot{\mathbf{x}}_d - \dot{\boldsymbol{\alpha}} + \mathbf{c}_2\boldsymbol{\lambda}_2 - \mathbf{B}\Delta\mathbf{u} \\ &= \mathbf{F}(\mathbf{x}_1, \hat{\mathbf{x}}_2) + \mathbf{B}(\mathbf{x}_1)\mathrm{sat}(\mathbf{u}) + \hat{\mathbf{D}} - \dot{\boldsymbol{\alpha}} + \mathbf{c}_2\boldsymbol{\lambda}_2.\end{aligned} \tag{47}$$

Then, the sliding surface (39) is rewritten as follows.

$$\mathbf{s} = \boldsymbol{\varphi}_1 + \mathbf{r}_1\,\mathrm{sgn}^{k_1}(\boldsymbol{\varphi}_1) + \mathbf{r}_2\,\mathrm{sgn}^{k_2}(\boldsymbol{\varphi}_2). \tag{48}$$

Differentiating Equation (48) and applying Equations (44) and (47), it yields

$$\begin{aligned}\dot{\mathbf{s}} &= \dot{\boldsymbol{\varphi}}_1 + k_1\mathbf{r}_1|\boldsymbol{\varphi}_1|^{k_1-1}\dot{\boldsymbol{\varphi}}_1 + k_2\mathbf{r}_2|\boldsymbol{\varphi}_2|^{k_2-1}\dot{\boldsymbol{\varphi}}_2 \\ &= -\mathbf{c}_1\boldsymbol{\varphi}_1 + \boldsymbol{\varphi}_2 + k_1\mathbf{r}_1|\boldsymbol{\varphi}_1|^{k_1-1}(-\mathbf{c}_1\boldsymbol{\varphi}_1 + \boldsymbol{\varphi}_2) + k_2\mathbf{r}_2|\boldsymbol{\varphi}_2|^{k_2-1}\dot{\boldsymbol{\varphi}}_2 \\ &= -\mathbf{c}_1\boldsymbol{\varphi}_1 - k_1\mathbf{r}_1\mathbf{c}_1\,\mathrm{sgn}^{k_1}(\boldsymbol{\varphi}_1) + \boldsymbol{\varphi}_2 + k_1\mathbf{r}_1|\boldsymbol{\varphi}_1|^{k_1-1}\boldsymbol{\varphi}_2 \\ &\quad + k_2\mathbf{r}_2|\boldsymbol{\varphi}_2|^{k_2-1}\left(\mathbf{F} + \mathbf{B}\mathbf{u} + \hat{\mathbf{D}} - \ddot{\mathbf{x}}_d - \dot{\boldsymbol{\alpha}} + \mathbf{c}_2\boldsymbol{\lambda}_2\right).\end{aligned} \tag{49}$$

Then, the control input of BNFTSMC method is designed as follows.

$$\mathbf{u} = \mathbf{B}^{-1}\left(-\boldsymbol{\rho}\mathbf{s} - \boldsymbol{\eta}\,\mathrm{sgn}(\mathbf{s}) - \mathbf{F} - \hat{\mathbf{D}} + \ddot{\mathbf{x}}_d + \dot{\boldsymbol{\alpha}} - \mathbf{c}_2\boldsymbol{\lambda}_2 - \frac{1}{k_2\mathbf{r}_2}|\boldsymbol{\varphi}_2|^{2-k_2}\left(1 + k_1\mathbf{r}_1|\boldsymbol{\varphi}_1|^{k_1-1}\right)\mathrm{sign}(\boldsymbol{\varphi}_2)\right), \tag{50}$$

where $\boldsymbol{\rho}$ is a positive definite diagonal matrix and $\boldsymbol{\eta}$ is a designed switching gain matrix.

Remark 11. The proposed BNFTSMC law combines the merits of the backstepping technique and NFTSMC method, such that the stratospheric satellite system can achieve singularity avoidance, strong robustness, and the fast finite-time convergence.

Theorem 12. *Considering the stratospheric satellite system subject to dynamic uncertainty and input saturation in Equation (15), if the NFTSM surface is selected as Equation (39). and the BNFTSMC controller is designed as Equation (50)., then the system is globally stable, and the tracking errors converge to zero in a finite time.*

Proof. Consider the following candidate Lyapunov function V_3

$$V_3 = V_2 + \frac{1}{2}\mathbf{s}^T\mathbf{s}. \tag{51}$$

□

Differentiating the above equation and applying Equations (46) and (49), the following relation can be computed.

$$\begin{aligned}\dot{V}_3 &= \dot{V}_2 + \mathbf{s}^T\dot{\mathbf{s}} \\ &= -\boldsymbol{\varphi}_1^T\mathbf{c}_1\boldsymbol{\varphi}_1 + \boldsymbol{\varphi}_1^T\boldsymbol{\varphi}_1 + \mathbf{s}^T\left(-\mathbf{c}_1\boldsymbol{\varphi}_1 - k_1\mathbf{r}_1\mathbf{c}_1\,\mathrm{sgn}^{k_1}(\boldsymbol{\varphi}_1) + k_2\mathbf{r}_2|\boldsymbol{\varphi}_2|^{k_2-1}(-\mathbf{k}\mathbf{s} - \boldsymbol{\eta}\,\mathrm{sgn}(\mathbf{s}))\right).\end{aligned} \tag{52}$$

Substituting Equation (48) into Equation (52), it follows

$$\begin{aligned}\dot{V}_3 &= -\boldsymbol{\varphi}_1^T\mathbf{c}_1\boldsymbol{\varphi}_1 + \boldsymbol{\varphi}_1^T\boldsymbol{\varphi}_2 + \mathbf{s}^T\left(-\mathbf{c}_1\boldsymbol{\varphi}_1 - k_1\mathbf{r}_1\mathbf{c}_1\,\mathrm{sgn}^{k_1}(\boldsymbol{\varphi}_1) + k_2\mathbf{r}_2|\boldsymbol{\varphi}_2|^{k_2-1}(-\mathbf{k}\mathbf{s} - \boldsymbol{\eta}\,\mathrm{sgn}(\mathbf{s}))\right) \\ &= -\boldsymbol{\varphi}_1^T\mathbf{c}_1\boldsymbol{\varphi}_1 + \boldsymbol{\varphi}_1^T\boldsymbol{\varphi}_2 + \left(\boldsymbol{\varphi}_1 + \mathbf{r}_1\,\mathrm{sgn}^{k_1}(\boldsymbol{\varphi}_1) + \mathbf{r}_2\,\mathrm{sgn}^{k_2}(\boldsymbol{\varphi}_2)\right)^T\left(-\mathbf{c}_1\boldsymbol{\varphi}_1 - k_1\mathbf{r}_1\mathbf{c}_1\,\mathrm{sgn}^{k_1}(\boldsymbol{\varphi}_1)\right) \\ &\quad - k_2\mathbf{r}_2|\boldsymbol{\varphi}_2|^{k_2-1}\left(\mathbf{s}^T\mathbf{k}\mathbf{s} + \mathbf{s}^T\boldsymbol{\eta}\mathbf{s}\right).\end{aligned} \tag{53}$$

Then, define a positive definite matrix $\mathbf{Q}$, which can be expressed as follows.

$$\mathbf{Q} = \begin{bmatrix} 2\mathbf{c}_1 + \mathbf{r}_1\mathbf{c}_1|\boldsymbol{\varphi}_1|^{k_1-1} + k_1\mathbf{r}_1\mathbf{c}_1|\boldsymbol{\varphi}_1|^{k_1-1} + k_1\mathbf{r}_1^T\mathbf{r}_1\mathbf{c}_1|\boldsymbol{\varphi}_1|^{k_1-1} & k_1\mathbf{r}_2^T\mathbf{r}_1\mathbf{c}_1|\boldsymbol{\varphi}_2|^{k_2-1} \\ -\mathbf{I}_{6\times6} & \mathbf{O}_{6\times6} \end{bmatrix}, \tag{54}$$

where $\|\mathbf{Q}\| = k_1\|\mathbf{r}_2^T\mathbf{r}_1\mathbf{c}_1|\boldsymbol{\varphi}_2|^{k_2-1}\| \geq 0$. Based on the above equation, $\dot{V}_3$ can be transformed into

$$\dot{V}_3 = -\begin{bmatrix}\boldsymbol{\varphi}_1^T & \boldsymbol{\varphi}_2^T\end{bmatrix}\mathbf{Q}\begin{bmatrix}\boldsymbol{\varphi}_1 \\ \boldsymbol{\varphi}_2\end{bmatrix} - k_2\mathbf{r}_2|\boldsymbol{\varphi}_2|^{k_2-1}\left(\mathbf{s}^T\mathbf{k}\mathbf{s} + \mathbf{s}^T\boldsymbol{\eta}\mathbf{s}\right) \leq 0. \tag{55}$$

On the basis of the Lyapunov stability theory, the system states $\boldsymbol{\varphi}_1$ and $\boldsymbol{\varphi}_2$ will asymptotically converge to the NFTSM surface $\mathbf{s}(t) = 0$. In order to demonstrate that the convergence occurs in finite time, let us introduce $\boldsymbol{\tau}_z$ and $\boldsymbol{\tau}_s$, which satisfy the following inequation.

$$\begin{aligned}-\begin{bmatrix}\boldsymbol{\varphi}_1^T & \boldsymbol{\varphi}_2^T\end{bmatrix}\mathbf{Q}\begin{bmatrix}\boldsymbol{\varphi}_1 \\ \boldsymbol{\varphi}_2\end{bmatrix} &\leq -\boldsymbol{\tau}_z^T|\boldsymbol{\varphi}_1|, \\ -k_2\mathbf{r}_2|\boldsymbol{\varphi}_2|^{k_2-1}\left(|\mathbf{s}|^T\mathbf{h} + |\mathbf{s}|^T\boldsymbol{\eta}\right)|\mathbf{s}| &\leq -\boldsymbol{\tau}_s^T|\mathbf{s}|.\end{aligned} \tag{56}$$

Continuously, Equation (55) can be rewritten as

$$\begin{aligned}\dot{V}_3 &= -\begin{bmatrix}\boldsymbol{\varphi}_1^T & \boldsymbol{\varphi}_2^T\end{bmatrix}\mathbf{Q}\begin{bmatrix}\boldsymbol{\varphi}_1 \\ \boldsymbol{\varphi}_2\end{bmatrix} - k_2\mathbf{r}_2|\boldsymbol{\varphi}_2|^{k_2-1}\left(|\mathbf{s}|^T\mathbf{h} + |\mathbf{s}|^T\boldsymbol{\eta}\right)|\mathbf{s}| \\ &\leq -\boldsymbol{\tau}_z^T|\boldsymbol{\varphi}_1| - \boldsymbol{\tau}_s^T|\mathbf{s}|.\end{aligned} \tag{57}$$

Table 2: Performance comparisons of different methods.

	Error	BSMC	BNFTSMC
IAE	$\boldsymbol{\zeta}_e$	2.1518×10^3	1.5368×10^3
	$\boldsymbol{\gamma}_e$	3.1345	1.2536
ITAE	$\boldsymbol{\zeta}_e$	2.2756×10^4	1.2484×10^4
	$\boldsymbol{\gamma}_e$	63.948	18.5927
ISE	$\mathbf{u}_v$	1.5467×10^{11}	1.3042×10^{11}
	$\mathbf{u}_\omega$	1.8409×10^{13}	1.0087×10^{13}

Considering the definition of Lyapunov function, Equation (57) can be converted to

$$\dot{V}_3 \leq -\sqrt{2}\boldsymbol{\tau}_z^T \frac{|\boldsymbol{\varphi}_1|}{\sqrt{2}} - \sqrt{2}\boldsymbol{\tau}_s^T \frac{|\mathbf{s}|}{\sqrt{2}}. \tag{58}$$

According to Lemma 5, define τ as the minimum element of the vector $[\sqrt{2}\boldsymbol{\tau}_z^T, \sqrt{2}\boldsymbol{\tau}_s^T]^T$, and we can get to

$$\begin{aligned} \dot{V}_3 &\leq -\sqrt{2}\boldsymbol{\tau}_z^T \frac{|\boldsymbol{\varphi}_1|}{\sqrt{2}} - \sqrt{2}\boldsymbol{\tau}_s^T \frac{|\mathbf{s}|}{\sqrt{2}} \\ &\leq -\tau \left(\left(\frac{|\boldsymbol{\varphi}_1|}{\sqrt{2}} \right)^2 + \left(\frac{|\mathbf{s}|}{\sqrt{2}} \right)^2 \right)^{1/2} = -\tau V_3^{1/2}. \end{aligned} \tag{59}$$

Thus, based on Lemma 4, the tracking error will converge to the equilibrium point in a finite time. Based on the analysis as mentioned above, the proposed control strategy is effective. Moreover, a flowchart of the observer-based robust finite-time controller design procedure is shown in Figure 3.

4. Simulation Results

In this section, numerical simulations of the trajectory tracking are carried out to confirm the effectiveness of the proposed observer-based robust finite-time control method. Also, for the purpose of comparison, "BNFTSMC" is used to represent the proposed controller. The physical parameters of the studied stratospheric satellite are adopted from Ref. [7]. Subsequently, to validate the performance of the designed strategy, backstepping sliding mode control (BSMC) method will be compared by simulations. The controller parameters of BNFTSMC are listed in Table 1.

The stratospheric satellite is initially located at $\boldsymbol{\zeta}_0 = [-40, 460, -19960]^T$(m), and its attitude is $\boldsymbol{\gamma}_0 = [0, 0, 0]^T$(rad). The initial body velocity and angular velocity are $\boldsymbol{\upsilon}_0 = [4.5, 0, 0]^T$(m/s) and $\boldsymbol{\omega}_0 = [0, 0, 0]^T$(rad/s). The limitations of the control inputs are $\mathbf{u}_{\boldsymbol{\upsilon},\max} = 10^4 \times [5, 5, 5]^T$, $\mathbf{u}_{\boldsymbol{\upsilon},\min} = -10^4 \times [5, 5, 5]^T$, $\mathbf{u}_{\boldsymbol{\omega},\max} = 10^5 \times [5, 5, 5]^T$, and $\mathbf{u}_{\boldsymbol{\omega},\min} = -10^5 \times [5, 5, 5]^T$. The time-varying disturbances, imposed on the stratospheric satellite, are given as:

$$\mathbf{D} = \begin{bmatrix} 0.1 + 0.05 \sin(0.1t) \\ 0.1 + 0.05 \sin(0.1t) \\ 0.1 + 0.05 \cos(0.1t) \\ 10^{-3} + 10^{-3} \sin(0.1t) \\ -10^{-3} + 10^{-3} \cos(0.1t) \\ 10^{-3} + 10^{-3} \sin(0.1t) \end{bmatrix}. \tag{60}$$

The desired trajectory is organized by circle in planar and helix in space, which is set as

$$\boldsymbol{\zeta}_d = \begin{bmatrix} 500 \sin(0.01t) \\ 500 \cos(0.01t) \\ -1t - 20000 \end{bmatrix} (\text{m}), \tag{61}$$

with the desired attitude calculated as

$$\boldsymbol{\gamma}_0 = \begin{bmatrix} \phi_d \\ \theta_d \\ \psi_d \end{bmatrix} = \begin{bmatrix} 0 \\ 0 \\ \arctan(\dot{y}_d, \dot{x}_d) \end{bmatrix} (\text{rad}). \tag{62}$$

The simulation results of the trajectory tracking with the proposed method are illustrated in Figures 4–17. The three-dimensional helical trajectory tracking results are presented in Figure 4, while the tracking results projected on x-z plane and y-z plane are shown in Figure 5. We can observe that the designed BNFTSMC method and BSMC method are capable of tracking the spiral trajectory even when the initial location is far from the reference trajectory. Figures 6 and 7 illustrate the position tracking responses and attitude tracking responses with disturbance inputs respectively. It is clear that the reference trajectory can be accurately tracked using the proposed BNFTSMC method within 40 s. From Figures 8 and 9, we can see that although BSMC strategy can track the predefined path, the tracking performance is not as good as the proposed method's, especially in aspects of tacking accuracy and convergence rate. The time histories of the linear velocity and angular velocity tracking responses are displayed in Figures 10 and 11. We can find that all the velocity changes of the designed controller are smoother and more continuous. The force inputs and torque inputs are shown in Figures 12 and 13. The green dotted line represents the predefined saturated constraints, and all control inputs are required to be within the limit of the actuator. It is worth noting that the control inputs of BSMC controller generate serious chattering on account of the existence of the designed saturation. Instead, the control forces and torques computed by the designed controller are smoother, and the chattering is effectively eliminated. Then, the observation errors of the system velocity states varying with time are presented in Figures 14 and 15. The proposed ESO holds the high estimation accuracies, which are on the order of 10^{-}

^{7}, 10^{-7}, 10^{-7}, 10^{-8}, 10^{-10}, and 10^{-11}. Additionally, it contributes to the high accuracy of the corresponding control law. Figures 16 and 17 show the disturbances along with their estimation of the ESO, in which we can see that the ESO can well approximate the external disturbance.

Furthermore, to illustrate the results more clearly and quantitatively, the integrated absolute error (IAE), the integrated time absolute error (ITAE), and the integral of square error (ISE) are introduced, which are defined as IAE = $\int_0^t |e(\tau)| \mathrm{d}\tau$, ITAE = $\int_0^t t|e(\tau)| \mathrm{d}\tau$, and ISE = $\int_0^t u(\tau)^2 \mathrm{d}\tau$. These performance indexes of the proposed method and BSMC method are computed to appraise the transient performance, the steady-state performance, and the control energy of the trajectory tracking controllers [7]. The performance comparisons of these methods are listed in Table 2. We can observe that, compared with BSMC method, the designed method results in the lower IAE and ITAE with consuming the smaller control energy and providing the better tracking performance.

5. Conclusion

An observer-based robust finite-time trajectory tracking control algorithm is presented for the stratospheric satellite subject to external disturbances and input saturation. Firstly, an ESO is adopted to be used for the observation of stratospheric satellite 6-DOF velocity and external disturbance. Then, the stability of the ESO is proven through theoretical derivation. The ESO provides the estimations of the unmeasurable states with high accuracy. Therefore, due to the ESO feedforward compensation to the controller, the chattering of the system is attenuated effectively. Then, a novel BNFTSMC strategy is proposed, where NFTSM surface is employed to guarantee the fast transient response and low tracking error, and backstepping technique is utilized to design the NFTSMC laws. Besides, the anti-windup technique is added to the control law to compensate for the saturation difference, which addresses the negative effect of the saturation problem. Then, based on the Lyapunov theory, the global stability and finite-time convergence are obtained. Finally, simulations are carried out to illustrate that the designed controller is effective and robust for tracking the reference trajectory with regard to the external disturbance and actuator saturation. Comparing results shows that the designed controller can provide high convergence rate and attenuate the chattering effect effectively without sacrificing the robustness of the controller.

Data Availability

The data that support the findings of this study are available from the corresponding author upon reasonable request.

Conflicts of Interest

The authors declare that there is no conflict of interest regarding the publication of this paper.

Acknowledgments

This research is funded by The Support Program of Young Talents of Huxiang (no. 2019RS2029), Chinese Postdoctoral Science Foundation (no. 47661), Youth Innovation Fund of Chinese High-Resolution Earth Observation Project, and High-Level Innovative Talent Program of NUDT.

References

[1] C. Nie, Z. Zheng, and M. Zhu, "Three-dimensional path-following control of a robotic airship with reinforcement learning," *International Journal of Aerospace Engineering*, vol. 2019, Article ID 7854173, 12 pages, 2019.

[2] Y. Yang, X. Xu, B. Zhang, W. Zheng, and Y. Wang, "Bionic design for the aerodynamic shape of a stratospheric airship," *Aerospace Science and Technology*, vol. 98, p. 105664, 2020.

[3] T. Zhang, S. Geng, X. Mu, J. Chen, J. Wang, and Z. Wu, "Thermal characteristics of a stratospheric airship with natural convection and external forced convection," *International Journal of Aerospace Engineering*, vol. 2019, Article ID 4368046, 11 pages, 2019.

[4] Z. Zuo, J. Song, Z. Zheng, and Q. L. Han, "A survey on modelling, control and challenges of stratospheric airships," *Control Engineering Practice*, vol. 119, p. 104979, 2022.

[5] Y. Yang, J. Wu, and W. Zheng, "Station-keeping control for a stratospheric airship platform via fuzzy adaptive backstepping approach," *Advances in Space Research*, vol. 51, no. 7, pp. 1157–1167, 2013.

[6] A. Parsa, S. B. Monfared, and A. Kalhor, "Backstepping control based on sliding mode for station-keeping of stratospheric airship," in *Proceedings of the 2018 6th RSI International Conference on Robotics and Mechatronics*, Tehran, Iran, 2018.

[7] Z. Zheng, M. Feroskhan, and L. Sun, "Adaptive fixed-time trajectory tracking control of a stratospheric airship," *ISA Transactions*, vol. 76, pp. 134–144, 2018.

[8] L. Sun and Z. Zheng, "Nonlinear adaptive trajectory tracking control for a stratospheric airship with parametric uncertainty," *Nonlinear Dynamics*, vol. 82, no. 3, pp. 1419–1430, 2015.

[9] Y. Yang, J. Wu, and W. Zheng, "Positioning control for an autonomous airship," *Journal of Aircraft*, vol. 53, no. 6, pp. 1638–1646, 2016.

[10] Y. Liu, A. Saeed, and M. Z. Shah, "Sliding mode lateral standoff tracking control of finless airship," *Aerospace Science and Technology*, vol. 119, p. 107164, 2021.

[11] X. Shao, J. Zhang, and W. Zhang, *Distributed Cooperative Surrounding Control for Mobile Robots with Uncertainties and Aperiodic Sampling*, IEEE Transactions on Intelligent Transportation Systems, 2022.

[12] J. Zhang, X. Shao, W. Zhang, and J. Na, *Path-Following Control Capable of Reinforcing Transient Performances for Networked Mobile Robots over a Single Curve*, IEEE Transactions on Instrumentation and Measurement, 2022.

[13] E. Paiva, F. Benjovengo, and S. Bueno, "Sliding mode control approaches for an autonomous unmanned airship," in *Proceedings of 18th AIAA lighter-than-air systems technology conference*, Washington, USA, 2009.

[14] Z. Zheng and L. Sun, "Adaptive sliding mode trajectory tracking control of robotic airships with parametric uncertainty and

wind disturbance," *Journal of the Franklin Institute*, vol. 355, no. 1, pp. 106–122, 2018.

[15] Y. Yang, J. Wu, and W. Zheng, "Trajectory tracking for an autonomous airship using fuzzy adaptive sliding mode control," *Journal of Zhejiang University SCIENCE C*, vol. 13, no. 7, pp. 534–543, 2012.

[16] Y. Wang, P. Zhou, J. A. Chen, and D. Duan, "Finite time attitude tracking control of an autonomous airship," *Transactions of the Institute of Measurement and Control*, vol. 40, no. 1, pp. 155–162, 2018.

[17] L. Cui, Y. Wei, and Y. Wang, "Finite-time trajectory tracking control for autonomous airships with uncertainties and external disturbances," *IET Intelligent Transport Systems*, vol. 14, no. 5, pp. 440–448, 2020.

[18] Y. Yang, "A time-specified nonsingular terminal sliding mode control approach for trajectory tracking of robotic airships," *Nonlinear Dynamics*, vol. 92, no. 3, pp. 1359–1367, 2018.

[19] Y. Yang, "Finite time positioning control for a stratospheric airship," *Advances in Space Research*, vol. 63, no. 8, pp. 2506–2514, 2019.

[20] Y. Yang and Y. Yan, "Neural network approximation-based nonsingular terminal sliding mode control for trajectory tracking of robotic airships," *Aerospace Science and Technology*, vol. 54, pp. 192–197, 2016.

[21] S. Lian, W. Meng, and Z. Lin, "Adaptive attitude control of a quadrotor using fast nonsingular terminal sliding mode," *IEEE Transactions on Industrial Electronics*, vol. 69, no. 2, pp. 1597–1607, 2021.

[22] N. Ali, I. Tawiah, and W. Zhang, "Finite-time extended state observer based nonsingular fast terminal sliding mode control of autonomous underwater vehicles," *Ocean Engineering*, vol. 218, p. 108179, 2020.

[23] Y. Miao, I. Hwang, M. Liu, and F. Wang, "Adaptive fast nonsingular terminal sliding mode control for attitude tracking of flexible spacecraft with rotating appendage," *Aerospace Science and Technology*, vol. 93, p. 105312, 2019.

[24] E. Liu, Y. Yan, and Y. Yang, "Neural network approximation-based backstepping sliding mode control for spacecraft with input saturation and dynamics uncertainty," *Acta Astronautica*, vol. 191, pp. 1–10, 2022.

[25] Y. Yang, "Positioning control for stratospheric satellites subject to dynamics uncertainty and input constraints," *Aerospace Science and Technology*, vol. 86, pp. 534–541, 2019.

[26] H. Gou, M. Zhu, Z. Zheng, X. Guo, W. Lou, and J. Yuan, "Adaptive fault-tolerant control for stratospheric airships with full-state constraints, input saturation, and external disturbances," *Advances in Space Research*, vol. 69, no. 1, pp. 701–717, 2022.

[27] S. Q. Liu, S. J. Gong, and Y. X. Li, "Vectorial backstepping method–based trajectory tracking control for an underactuated stratospheric airship," *The Aeronautical Journal*, vol. 121, no. 1241, pp. 916–939, 2017.

[28] J. Yuan, M. Zhu, X. Guo, and W. Lou, "Finite-time trajectory tracking control for a stratospheric airship with full-state constraint and disturbances," *Journal of the Franklin Institute*, vol. 358, no. 2, pp. 1499–1528, 2021.

[29] T. Chen, M. Zhu, and Z. Zheng, "Asymmetric error-constrained path-following control of a stratospheric airship with disturbances and actuator saturation," *Mechanical Systems and Signal Processing*, vol. 119, pp. 501–522, 2019.

[30] Z. Zheng and L. Sun, "Error-constrained path-following control for a stratospheric airship with actuator saturation and disturbances," *International Journal of Systems Science*, vol. 48, no. 16, pp. 3504–3521, 2017.

[31] Z. Zheng and L. Xie, "Finite-time path following control for a stratospheric airship with input saturation and error constraint," *International Journal of Control*, vol. 92, no. 2, pp. 368–393, 2019.

[32] Y. Wang, W. Zhou, J. Luo, H. Yan, H. Pu, and Y. Peng, "Reliable intelligent path following control for a robotic airship against sensor faults," *IEEE/ASME Transactions on Mechatronics*, vol. 24, no. 6, pp. 2572–2582, 2019.

[33] W. Zhang, X. Shao, W. Zhang, J. Qi, and H. Li, "Unknown input observer-based appointed-time funnel control for quadrotors," *Aerospace Science and Technology*, vol. 126, p. 107351, 2022.

[34] A. S. S. Abadi, P. A. Hosseinabadi, and S. Mekhilef, "Fuzzy adaptive fixed-time sliding mode control with state observer for a class of high-order mismatched uncertain systems," *International Journal of Control, Automation and Systems*, vol. 18, no. 10, pp. 2492–2508, 2020.

[35] K. Gong, Y. Liao, and Y. Mei, "Extended state observer–based output feedback control for spacecraft pose tracking with control input saturation," *Proceedings of the Institution of Mechanical Engineers, Part G: Journal of Aerospace Engineering*, vol. 236, no. 4, pp. 645–660, 2022.

[36] W. Perruquetti, T. Floquet, and E. Moulay, "Finite-time observers: application to secure communication," *IEEE Transactions on Automatic Control*, vol. 53, no. 1, pp. 356–360, 2008.

[37] R. Meng, S. Chen, C. Hua, J. Qian, and J. Sun, "Disturbance observer-based output feedback control for uncertain QUAVs with input saturation," *Neurocomputing*, vol. 413, pp. 96–106, 2020.

[38] Z. Xu, X. Yang, W. Zhang, W. Zhang, L. Zhang, and P. X. Liu, "Backstepping sliding mode control based on extended state observer for robotic manipulators with LuGre friction," *International Journal of Control, Automation and Systems*, vol. 20, no. 6, pp. 2054–2066, 2022.

[39] H. K. Khalil, *Nonlinear Control*, Pearson, press, 2015.

[40] S. P. Bhat and D. S. Bernstein, "Geometric homogeneity with applications to finite-time stability," *Mathematics of Control, Signals, and Systems*, vol. 17, no. 2, pp. 101–127, 2005.

[41] Y. Yang, J. Wu, and W. Zheng, "Design, modeling and control for a stratospheric telecommunication platform," *Acta Astronautica*, vol. 80, pp. 181–189, 2012.

[42] M. Boukattaya, N. Mezghani, and T. Damak, "Adaptive nonsingular fast terminal sliding-mode control for the tracking problem of uncertain dynamical systems," *ISA Transactions*, vol. 77, pp. 1–19, 2018.